Accepted Manuscript

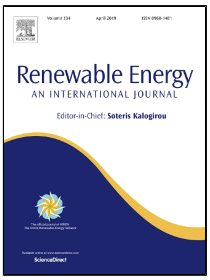

Parametric Investigation of Traditional Vaulted Roofs in Hot-Arid Climates

Amira Elnokaly, Mohammed Ayoub, Ahmed Elseragy

PII:	S0960-1481(19)30061-8
DOI:	10.1016/j.renene.2019.01.061
Reference:	RENE 11062
To appear in:	*Renewable Energy*
Received Date:	17 February 2017
Accepted Date:	15 January 2019

Please cite this article as: Amira Elnokaly, Mohammed Ayoub, Ahmed Elseragy, Parametric Investigation of Traditional Vaulted Roofs in Hot-Arid Climates, *Renewable Energy* (2019), doi: 10.1016/j.renene.2019.01.061

Parametric Investigation of Traditional Vaulted Roofs in Hot-Arid Climates

Amira Elnokaly
Associate Professor (Principal Lecturer), School of Architecture and the Built Environment
University of Lincoln
Email: aelnokaly@lincoln.ac.uk
United Kingdom

Mohammed Ayoub (Corresponding Author)
Associate Professor, Architectural Engineering and Environmental Design Department
Arab Academy for Science and Technology and Maritime Transport, Alexandria, Egypt
Abou Keer, Alexandria, Egypt. P.O. Box 1029
Email: dr.ayoub@aast.edu
Telephone Number: +20-122-3691802

Ahmed Elseragy
Professor, Architectural Engineering and Environmental Design Department
Arab Academy for Science and Technology and Maritime Transport, Alexandria, Egypt
Email: ahmed.elseragy@yahoo.co.uk
Egypt

Abstract

In the Mediterranean and North African regions, traditional vaulted roof forms have been widely used due to their significant influence on enhancing thermal indoor conditions. This research parametrically investigates the thermal performance of vaulted roofs, seeking a better understanding of the reciprocal relationship between the solar irradiance received by these roofs and the resulting energy consumption in the hot-arid city of Aswan (23.58°N), Egypt. The methodological procedure is realized through two phases. The annual simulations of solar irradiance and energy consumption are carried out in the first phase, where the quantitative performance of 2,310 different cases are predicted in terms of six vaulted roof forms against eleven key influencing variables. The unsupervised technique of Principal Component Analysis is used in the second phase to reduce the higher dimensionality of the resulting dataset and extract important information from newly established orthogonal principal components. The outcomes of this work aim to provide architects and practitioners with an optimized dataset to use in the design and application of vaulted roof forms and support decision makers addressing the development strategies by providing essential data for setting regulations of newly built environments in harsh hot-arid contexts.

Key Words: Solar Irradiance; Energy Consumption; Vaulted Roofs; Parametric Approach; Principal Component Analysis.

Parametric Investigation of Traditional Vaulted Roofs in Hot-Arid Climates

Abstract

In the Mediterranean and North African regions, traditional vaulted roof forms have been widely used due to their significant influence on enhancing thermal indoor conditions. This research parametrically investigates the thermal performance of vaulted roofs, seeking a better understanding of the reciprocal relationship between the solar irradiance received by these roofs and the resulting energy consumption in the hot-arid city of Aswan (23.58^{o}N), Egypt. The methodological procedure is realized through two phases. The annual simulations of solar irradiance and energy consumption are carried out in the first phase, where the quantitative performance of 2,310 different cases are predicted in terms of six vaulted roof forms against eleven key influencing variables. The unsupervised technique of Principal Component Analysis is used in the second phase to reduce the higher dimensionality of the resulting dataset and extract important information from newly established orthogonal principal components. The outcomes of this work aim to provide architects and practitioners with an optimized dataset to use in the design and application of vaulted roof forms and support decision makers addressing the development strategies by providing essential data for setting regulations of newly built environments in harsh hot-arid contexts.

Key Words: Solar Irradiance; Energy Consumption; Vaulted Roofs; Parametric Approach; Principal Component Analysis.

Introduction

In Egypt, almost 42% of energy is consumed by the buildings sector (EMEE, 2012), with more than 90% of its generated electricity from non-renewable resources (Atlam and Rapiea, 2016). Climate change causes a steep increase in air temperature due to heat waves, coupled with a continuous use of HVAC systems that only surged the energy demand. These expanded the anthropogenic polluted heat, and in turn, the urban heat island. Last two decades, the Egyptian residential building sector have witnessed a stressed electricity demand, with a steady increase annually (Mourtada, 2009). Today, the predominant character of the major Egyptian cities manifests repetitions of minimalistic, identical, underlit, and unventilated residential blocks (Fahmy, 2010). Also, many passive design techniques of the Egyptian traditional architecture have vanished, particularly passive cooling strategies that prevents against overheating in the indoor built environment (Santamouris and Asimakopoulos, 1996). Such factors have accelerated the reliance on air conditioners and mechanical acclimatization allover Egypt, resulting in high rates of energy consumption that cannot be converged by electricity-generating capacity (EERA, 2014). For that very reason, the strategic objectives of the Egyptian Residential Energy Code's (EREC) directed stakeholders towards utilizing energy conservation techniques in buildings designs (EERA, 2014). Some of the main concepts EREC identifies is the 'building envelope' and its thermal insulation that are recommended to reduce heat gain and hence energy consumption by controlling the heat flow in and out of the building (Okba, 2005; Attia, 2010; AlQadi, et al., 2018). To achieve higher comfort levels, traditional architecture incorporated varied aspects such as natural ventilation, shading, thermal mass and passive cooling techniques as some of the most important features in Egyptian traditional architecture (Fathy, 1986; Elnokaly and Elseragy, 2013). In hot-arid climate regions, 70-80% of total energy consumption is used to operate active cooling systems (Koch-Nielsen, 2013), and consequently, reducing the reliance on those will have a drastic impact on energy consumption. An optimized envelope design can improve the thermal performance through passive solar techniques (Fahmy, et al., 2015), and the building roofs has a deep role to play in this process (Ayoub and Elseragy, 2018). Limitations in understanding environmental and thermal performances of architectural geometries have to some extent hindered their acceptance by clients and the building industry (Elseragy and Elnokaly, 2007). Since roofs receive the highest amount of solar irradiance, causing overheating in this climate (Elnokaly and Elseragy, 2006), the indoor thermal comfort depends on reducing this solar intensity without the reliance on mechanical devices (Elseragy and Gadi, 2003a; 2003b; Elseragy and Elnokaly, 2007). There are other variables that influence indoor thermal comfort such as thermos-physical properties of the building's envelope material (Zeng et al, 2011); the roof optical properties, namely the albedo, thermal emissivity and the roof insulation (Ramamurthya et al, 2015; Santamouris et al, 2011; Meyn and Oke, 2009) that was demonstrated to play a very important role in the energy balance of buildings (Costanzo, 2013). However, this study mainly examines the impact of various geometrical forms of vaulted roofs, as part of the building envelope elements, on indoor thermal behavior under different conditions in hot-arid climate of Egypt. Vaults and domes are useful treatments used in the traditional architecture to adapt with the hot-arid climate. These traditional curved forms have many

advantages reducing the total heat gain from the roof and providing a passive cooling effect for buildings by increasing the height of the space, and consequently, warm air rises far above the occupants, as heat is lost by convective ventilation through certain roof openings to the outdoors (Fathy, 1986).

Review of Vaulted and Domed Roofs

Qualitative explanations were previously presented on the ability of curved roofs in hot-arid regions to maintain lower indoor temperatures during the hot summer and reflect more solar radiation, compared to flat roofs (Fathy, 1986; Bowen, 1981; Koita, 1981). Nevertheless, many of them were provided without factual or empirical data. In spite their logic, further quantifications are required to investigate their ability to mitigate undesirable environmental conditions. In one of earlier studies, Olgyay (1973) showed that the lower indoor air temperature of curved roof buildings is due to the lower absorbed solar radiation, compared to flat roofs. His findings were later confirmed by Konya (1980). Mainstone (1983) claimed that the reason behind this is due to higher ground and sky reflected radiation heat loss. However, it was not until 1990s when Pearlmutter (1993) conducted the first attempt to quantitatively compare the thermal behaviour of vaulted roof forms (VRFs) against flat roofs in terms of indoor temperatures. His study revealed the ability of VRFs to offer greater thermal stability, providing favorable daytime temperature. Following this work, only few studies have used empirical methods to explore the impact of various VRFs (Elseragy, 2003; Elseragy and Gadi, 2003b; Elseragy and Elnokaly, 2007). Elseragy (2003) established a theoretical basis of these claims and validated the thermal advantages of curved roof forms in hot-arid regions. He tested both the vaulted and domed roofs with various inclinations and orientations and provided a mathematical model for measuring the solar irradiance on tilted/curved surfaces. Semi-circular domes were examined by Gómez-Muñoz et al. (2003) who validated Elseragy's work. Elseragy (2003) identified "self-shading" property as an advantage of curved roofs, which was agreed by Gómez-Muñoz et al. (2003) and referred to as "auto shading." Later, this advantage was also confirmed by Hadavand and Yaghoubi (2008). While many researches put the focus on other climate-related issues, Tang et al. (2003a and 2003b) asserted that the use of curved roofs in contemporary architecture of hot-arid regions has yet to be explored on their influence of solar radiation and heat transfer. Other researchers investigated the use of domed roofs but very little is done on VRFs. Faghih and Bahadori (2011) studied the performance of domed roofs, considering air flow, solar radiation, and heat transfer. They revealed that domed roofs outperform flat roofs on warm days, especially the domes covered with glazed tiles. In certain cases, they found that wind flow direction and speed are not essential in decreasing room temperature of the domed roofs. Soleimani et al. (2016) conducted a computational simulation of the wind-induced ventilation in a geodesic dome in a hot climate. They reported that natural ventilation by upper roof openings can reduce the indoor air temperature during winter periods. During hot summer periods, however, this technique cannot satisfy thermal requirements, in accordance with Faghih and Bahadori (2011) results, recommending that complementary cooling solutions should be considered. Some other researchers considered the impact of the external form of the building on energy consumption, as in the work of Zerefos et al. (2012), while others studied the thermal

performance of tilted/curved roof forms. Sirimanna and Attalage (2016) conducted a study on buildings in the Mediterranean region, where they concluded that the external form of a building has a great impact on energy consumption despite of the materials and its usage. Tilted/curved roof geometries of high angles of incidence from solar radiation are advantageous than flat ones in energy consumption reduction, hence, cooling loads are reduced. In a recent study, Ayoub and Elseragy (2018) confirmed the ability of domed roofs to significantly decrease the received solar irradiance in comparison to flat roof surfaces throughout the year. However, they only considered domed roof forms rather VRFs. Though interesting findings, the collective conclusions of the reviewed studies suggest that an additional work should put the focus on expanding the investigations to fully comprehend the thermal behaviour of VRFs against different variables on an annual basis with reference to hot-arid climates. In addition, no researches on these techniques have been conducted for VRFs in Aswan.

Vaulted Roof Forms

Geometrically, there is a wide variety of vaults (Figure 1), which are arched forms used to provide spaces with a ceiling or roof. Vaults apply lateral load that requires continuous walls of a significant thickness as counter load-resisting elements. The simplest kind of a vault is the Barrel Vault, resembling a continuous semicircular arch, where the length is usually greater than or equal to its diameter. A variety of a Barrel Vault is the Pointed Vault, which has been widely employed because of its greater strength and reduced load applied on the walls. Another example is the intersecting barrel vault, or the Groin Vault. It is used for spaces of great dimensions, where two semicircular barrel vaults of the same diameter cross each other. Their intersection is an ellipse that is known as a groin, down which the load of the vault is carried to the cross walls. A diversiform of Groin Vault is the Pointed Groin Vault, where its own weight is applied more directly downward than the groin vault, requiring less thick walls as counter load-resisting elements, and in turn, allows for larger openings beneath the outer rips. Another type of vaults is the domical vault or Cloister Vault that consists of four concave surfaces meeting at a curve, or a point in the case of Pointed Cloister Vault, above its center. The Cloister Vault is the intersection of the space beneath two barrel or pointed vaults perpendicular to each other. In this way, it differs from a Groin Vault that is also formed by two barrel or pointed vaults perpendicular to each other, yet a Cloister Vault is the union of spaces beneath them.

Aim of the Study

This research addresses the question of achieving indoor thermal comfort by integrating the traditional VRFs into contemporary buildings in Aswan, Egypt. The parametric approach is utilized to investigate the solar irradiance received by these roofs along with the resulting energy consumption of several VRFs by means of computational simulations of the Average Hourly Total Irradiance (AHTI) (kWh/m^2), and the resulting Average Hourly Energy Consumption (AHEC) (kWh/m^2) for potential cooling loads. This approach reflects a mediation to an existing situation that is associated with hot-arid environments, to ultimately improve the indoor environmental quality. Several empirical equations verified that at the same

geographical latitude, solar irradiance received by a surface differs significantly according to its geometrical configuration, form, orientation, and other related variables (Elseragy and Gadi, 2003a; Elseragy and Elnokaly, 2007). This signifies the necessity to investigate different VRFs against a number of these influencing variables.

Methodology

The methodological procedure includes identifying the simulations tools and settings of solar irradiance and energy consumption. The reference residential study model and its key influencing variables are then described, on which the simulations are conducted. The calculations of solar irradiance and the resulting energy consumption would require conducting annual simulations on an hourly-basis with regard to the selected geographic location. Herein, this parametric study is realized through two phases. The first phase utilizes an algorithm that derives a number of pre-defined variables to model and simulate different VRFs. This will reveal their quantitative performance against these variables through the computational simulations, concluding VRFs that receive lower solar irradiance, and consequently, yield less energy consumption. However, the increased number of the study variables makes it difficult to comprehend the relationships between them, even with traditional statistical techniques. The objective of the second phase is to reduce the higher dimensionality of the dataset resulted from the first phase, revealing fewer variables to consider. This can be achieved by Principal Component Analysis (PCA), which converts a multivariate dataset into uncorrelated variables, representing a combination of the original variables. The dimensionality reduction is achieved by considering the most important components that hold as much information as possible of the original dataset. The quantitative measurements of this work will provide an extensive set of data to be used by architects, planners, and policy makers in the building industry.

Simulation Tools and Settings

In this study, Rhinoceros's Grasshopper developed by David Rutten at Robert McNeel and Associates (Tedeschi and Andreani, 2014), is used to create different 3D models of VRFs. It is a graphical algorithm editor that supports the associative parametric approach (Ayoub, 2016). Grasshopper runs under Rhinoceros 3D modeling platform, which is a NURBS-based 3D modeling platform commonly used in industrial design, architecture, and other multimedia and graphic designs (Becker and Golay, 1999). The solar irradiance and energy simulations are performed using Diva-for-Rhino (Jakubiec, and Reinhart, 2011), developed by Solemma LLC: Environmental analysis for buildings, while the energy simulations are conducted using Archsim by Timur Dogan (Dogan et al., 2014). Diva-for-Rhino is a plug-in for Rhinoceros that interfaces Radiance (Ward, 1994), a validated engine for daylighting and solar irradiance simulations (Lagios et al., 2010; Jakubiec, and Reinhart, 2011; Costanzo et al., 2018). It creates a continuous cumulative sky radiance map distribution method called GenCumulativeSky, in which it is significantly faster with a minimal sacrifice in accuracy compared to other methods (Robinson and Stone, 2004). Archsim Energy Modeling is a multi-zone energy simulation tool that interfaces the validated EnergyPlus engine for

energy simulations (Winkelmann, 2001). The EnergyPlus operates in compliance with the ANSI/ASHRAE Standard 140-2011 Standard Method of Test for the Evaluation of Building Energy Analysis Computer Programs (ANSI/ASHRAE Standard 140, 2011). As a part of the DIVA-for-Rhino analysis suite, Archsim's energy consumption predictions are seamlessly combined with DIVA-for-Rhino's solar irradiance calculations (Jakubiec and Reinhart, 2011). The investigations consider the simulation run period to be annually based on hourly resolution. The effect of solar irradiance is undetectable during nocturnal hours, they were added to the results dataset, since the residential space may have different characteristics of energy consumption during these hours. The simulation settings are consistent to Aswan's (23.58°N) Typical Meteorological Year (TMY) weather data file. Radiance and EnergyPlus parameters are shown in (Table 1). Each generated roof geometry is divided into discrete counterparts. The discretization size, or grid spacing, is set to be 0.45 m, which is less than LEEDv4 requirement of 0.60 m (USGBC, 2019). DIVA-for-Rhino actually calculates the number of divisions that closely matches the input grid size, thus, it's more of an average than an exact number. This step is usually carried out to construct counterparts suitable for analysis and implementation of computational investigations of solar irradiance in DIVA-for-Rhino.

Table 1: Computational Simulations Settings

Computational Investigations Settings	
Location	Aswan, Egypt (23.58°N)
Study Period	Annual with and Hourly Resolution
Analysis Grid Size	0.45
Radiance Parameters	
Ambient Accuracy (aa)	0.15
Ambient Bounce (ab)	6
Ambient Division (ad)	1024
Ambient Resolution (ar)	256
Ambient Sampling (as)	128
EnergyPlus Parameters	
People	0.20 Person/m^2
Lighting	12 W/m^2
Cooling Setpoint Temperature	26°c
Electrical Equipment, Mechanical Ventilation, and Hot Water	No

Reference Residential Study Model (RRSM)

The developed algorithm by the authors is utilized to generate the Reference Residential Study Model (RRSM). It represents a domestic residential space located at the ground floor that reflects different orientations and other geometrical configurations of VRFs. The RRSM is covered by a variable VRF to receive the solar irradiance, in which its form is manipulated by a range of variable Cross-Sectional Ratio from 0.00 to 2.00 (Figure 2), and orientations from 0° to 180° with an increment 45° counterclockwise. The RRSM parameters, configurations, and materials (Table 2) are meant to act as a baseline for the computational investigations in the first phase. The wall and roof sections for the thermal model are selected according to the optimized case for the Egyptian typical wall section for the residential sector, assuming to coincide with the Egyptian Code for Energy Efficiency in Residential Buildings, ECP 306-2005 - First Section (306/1) (EERB, 2008). In this case, the energy simulations are instructed to calculate cooling

energy only and consider the effect of thermal transmittance through walls and roofs, while floor are set to be adiabatic. The total U-value of the external wall is 0.34 W/m^{2}K, and the external roof is 0.48 W/m^{2}K, retrieved with modification from (Attia, and Wanas, 2012). The energy simulation discards internal heat gains from any electrical equipment, mechanical ventilation, and hot water, to focus the energy consumption due to VRFs only. Screens of RRSM are represented as horizontal strips, co-planar with each wall to eliminate the effect of opening orientation. The centers of the screens are aligned to 50% of the wall height, with equal sills and lintels of 1.00 m.

Table 2: RRSM Parameters, Configurations, and Materials

Reference Residential Study Model (RRSM) Parameters	
Base Level	Ground floor level
Width	10.00, 7.50, and 5.00 m
Length	10.00, 7.50, and 5.00 m
Height	3.00 m
Roof/RRSM Width x Length Combinations	10.0x10.0, 10.0x7.5, 10.0x5.0, 7.5x5.0, 7.5x10.0, 5.0x10.0, and 5.0x7.5 Combined with Heights (from 0 to 10) with 77 Combinations in Total.
Surfaces Materials	
Walls	30% reflectance
Roof	20% reflectance
Glazing	88% visual transmittance
Screen Parameters	
Glazing	Single Panel Clear Glazing, Thickness=6 mm
Window Frame	Wooden Frame of 5 cm without any dividers
Screen Dimensions	Horizontal Stripes on each wall Sill=1.00 m, Lintel=1.00 m
Screen Glazing Material	U-value=5.778, SHGC=0.819, TSOL=0.775, TVIS=0.881

SHGC: Solar Heat Gain Coeff.; **TSOL**: Solar Transmittance Coeff.; **TVIS**: Visible Transmittance Coeff.

Key Influencing Variables and Parametric Algorithm

The accumulations of the previously reviewed researches examined a number of related factors with the intention of quantitatively comparing thermal behaviour of VRFs. They showed that the enhancement of solar irradiance levels and energy consumption are significantly affected by numerous key variables, related to the geometry of VRFs. This suggests a derived rule-of-thumb is hard to acquire, yet the investigation of these variables of VRFs would explain the relationship between roof geometries and the received solar irradiance along with the resulting energy consumption. The key influencing variables and their associated ranges are shown in (Table 3). They are investigated through a multiple simulation process, where the computational investigations simulations calculate the AHTI and AHEC for each VRF considering the specified ranges of the influencing variables. These variables are considered independent variables, while AHTI and AHEC are dependent variables. The total number of simulation runs is: 6 VRFs x 5 RRSM Orientations x 77 VRFs/RRSM Combinations = 2,310.

Table 3: The Key Influencing Variables and their Associated Ranges

No.	Key Influencing Variables	Unit	Minimum	Maximum
1	Rotational Angle	Degrees	0.00	180.00
2	Roof Height	m	0.00	10.00
3	Roof/RRSM Width	m	5.00	10.00
4	Roof/RRSM Length	m	5.00	10.00

5	RRSM Internal Area	m^2	25.00	100.00
6	RRSM Internal Volume	m^3	75.00	1065.27
7	Thermal Envelope: Sum of External Walls and Roof Total Area	m^2	110.00	613.33
8	Roof External Area	m^2	25.00	240.28
9	Roof Aspect Ratio: Length/Width	-	0.5	1.00
10	RRSM Compactness Ratio: Thermal Envelope/Volume	m^{-1}	1.46	0.57
11	Roof Cross-Sectional Ratio: Height/Width	-	0	2

In Grasshopper's computational environment, the authors developed an algorithm to derive the simulations for large number of VRFs (Figure 1) with varying configurations and orientations. It utilizes the parametric methodology through numerical inputs, geometric transformations, mathematical formulas, and logical relationships. Grasshopper is used to automate the overall process (Figure 3). The modeling of VRFs basically consists of two curves lofted together to create different vaults according to the defined VRFs/RRSM variables shown in (Table 2) and (Table 3). By manipulating these variables using brute-force exhaustive search, numerous 3D models are generated, each of which Grasshopper sends to Diva-for-Rhino and Archsim for the simulation and calculation of AHTI and AHEC respectively based on the simulation settings (Table 1). The AHTI and AHEC values are then sent back to Grasshopper, where it is used this time to collect the results of each run along with their corresponding inputs variables. Grasshopper then exports the resulting dataset to Microsoft Excel for further analysis and representation.

Results and Discussion

The first subsection illustrates the simulation results of AHTI and AHEC in terms of the 11 key influencing variables. In addition, it presents the processing of the subsequent data to conclude the optimal VRFs configurations that yield minimized solar irradiance with less energy consumption. Following, the second subsection shows the steps of the developed PCA to reduce the higher dimensionality of the resulting dataset including the charts of the established principal components.

The First Phase: Evaluation of Solar Irradiance and Energy Consumption

Using Diva-for-Rhino and Archsim, the annual solar irradiance and energy consumption simulations are conducted for each VRF configuration. The simulation and data extraction process took approximately 270 hours on an Intel i7-4790K CPU, with installed memory (RAM) of 16.0 GB, and 64-bit operating system. To offer a comprehensive visualization of the simulation runs against the influencing variables, a parallel coordinates plot (Figure 4) is drawn where the variables are represented on 11 vertical and equally spaced parallel axes. This plot contains additional two axes for the resulting AHTI and AHEC. It displays the simulation runs as polylines in the 11-dimensional experiment space, where each variable value is represented by a point on a polyline. This makes parallel coordinate plots similar in appearance to line charts, but the way data is translated into a plot is substantially different. The slopes of the line charts indicate the change from one value to another, as the polylines connect a series of values each associated with a different variable measure. The scales of these variables are standardized to range from of 0.0 of 1.0. This visualization is an effective technique to plot many variables together along with the relationships

between them, when it is difficult to visualize complicated datasets of higher dimensionality. In order to review and explain the simulation results, they must be processed first, allowing to handle larger datasets with the available computational power. The data-processing of simulation results includes a number of steps. After extracting the hourly results from Grasshopper to Microsoft Excel and arranging them in a tabular format, they are converted into monthly average hourly data: $AHTI_{Monthly}$ and $AHEC_{Monthly}$. These new metrics are derived from the original datasets by calculating the average hourly observations in a given month. For each VRF, the $AHTI_{Monthly}$ addresses all the first hour observations of each day in a given month and calculates their monthly average hourly solar irradiance. Then it takes all the second hour observations of each day in the same month and calculates its average, and so on. This procedure is repeated for all months of the year. Likewise, $AHEC_{Monthly}$ addresses each hour of each day in a given month and calculates its energy consumption monthly average hourly. For each VRF, these results in 288 data entries consisting of 24 hours per 12 months. In order to test the similarity and association between the original hourly AHTI and AHEC and the newly generated $AHTI_{Monthly}$ and $AHEC_{Monthly}$, a two tailed t-test is performed to compare the means and variances of the two continuous datasets for all the study's VRFs. There are two hypotheses to test here, the Null Hypothesis H_0: where there is no difference between the two datasets, and the Alternate Hypothesis H_1: in which there is a difference between the two datasets. As shown in (Table 4-a) and (Table 4-b), all VRFs yielded smaller t-stat values than their corresponding two tail t-critical values confirming the rejection of the alternate hypothesis in favour of the null hypothesis. Additionally, the t-test results showed an association between the two datasets, where their p-values are considerably larger than the significance level of 0.05. Therefore, there is enough evidence to support the null hypothesis and to reject the alternative hypothesis. There is no statistical difference between the two datasets, and the original dataset is well represented in the new one.

Table 4-a: Example of Barrel VRF (Rotational Angle = 0.00) with their Corresponding Roof Widths, Lengths, and Heights showing the Two Tailed t-test Results for the AHTI and $AHTI_{Monthly}$.

Roof Config.		t-stat	t-critic.	p-value	Original Dataset Mean	Original Dataset Variance	Monthly Dataset Mean	Monthly Dataset Variance
W x L	H							
10.00x10.00	0	0.0078	1.9602	0.9938	248.0457	133408.94	247.8756	117575.00
	1	0.0093	1.9602	0.9926	251.5160	145603.38	251.3040	133717.12
	2	0.0101	1.9602	0.9920	231.9139	137359.56	231.6905	129030.89
	...	...	...	...	...	...	...	...
	8	0.0096	1.9602	0.9924	142.3363	68079.35	142.1867	64097.66
	9	0.0097	1.9602	0.9923	140.6427	66887.47	140.4934	62952.08
	10	0.0096	1.9602	0.9924	139.3040	65986.04	139.1567	62096.67
10.00x07.50	0	0.0078	1.9602	0.9938	248.0457	133408.94	247.8756	117575.01
	1	0.0093	1.9602	0.9926	251.5229	145611.83	251.3110	133725.92
	2	0.0101	1.9602	0.9920	231.9137	137359.33	231.6904	129030.65
	...	...	...	...	...	...	...	...
	8	0.0096	1.9602	0.9924	142.3363	68079.36	142.1867	64097.67
	9	0.0097	1.9602	0.9923	140.6427	66887.47	140.4934	62952.08
	10	0.0096	1.9602	0.9924	139.3040	65986.04	139.1567	62096.67
05.00x10.00	0	0.0078	1.9602	0.9938	248.0457	133408.94	247.8756	117575.01
	1	0.0101	1.9602	0.9920	231.9426	137402.26	231.7191	129073.87
	2	0.0101	1.9602	0.9919	166.1697	86683.27	165.9910	81946.48
	...	...	...	...	...	...	...	...

	8	0.0095	1.9602	0.9925	135.1751	62908.13	135.0332	59131.13
	9	0.0094	1.9602	0.9925	134.1172	62369.85	133.9766	58628.90
	10	0.0094	1.9602	0.9925	133.2559	61793.57	133.1156	58071.02
05.00x07.50	0	0.0078	1.9602	0.9938	248.0457	133408.94	247.8756	117575.01
	1	0.0101	1.9602	0.9920	231.9424	137402.01	231.7189	129073.61
	2	0.0101	1.9602	0.9919	166.1697	86683.27	165.9910	81946.48
	...	...	...	...	...	...	...	...
	8	0.0095	1.9602	0.9924	134.8370	62853.41	134.6948	59083.29
	9	0.0094	1.9602	0.9925	134.1493	62324.37	134.0086	58582.29
	10	0.0094	1.9602	0.9925	133.2559	61793.57	133.1156	58071.02

Table 4-b: Example of Barrel VRF (Rotational Angle = 0.00) with their Corresponding Roof Widths, Lengths, and Heights showing the Two Tailed t-test Results for the AHEC and $AHEC_{Monthly}$

Roof Config. W x L	H	t-stat	t-critic.	p-value	Original Dataset Mean	Original Dataset Variance	Monthly Dataset Mean	Monthly Dataset Variance
10.00x10.00	0	0.1116	1.9602	0.9112	0.0584	0.0002	0.0583	0.0002
	1	0.1124	1.9602	0.9105	0.0585	0.0002	0.0584	0.0002
	2	0.1134	1.9602	0.9097	0.0587	0.0002	0.0586	0.0002
	...	...	...	...	...	...	...	...
	8	0.1196	1.9602	0.9048	0.0604	0.0003	0.0603	0.0003
	9	0.1202	1.9602	0.9043	0.0607	0.0003	0.0605	0.0003
	10	0.1209	1.9602	0.9038	0.0609	0.0004	0.0608	0.0003
10.00x07.50	0	0.1095	1.9602	0.9128	0.0607	0.0002	0.0606	0.0002
	1	0.1106	1.9602	0.9119	0.0608	0.0002	0.0607	0.0002
	2	0.1119	1.9602	0.9109	0.0610	0.0002	0.0609	0.0002
	...	...	...	...	...	...	...	...
	8	0.1190	1.9602	0.9053	0.0631	0.0004	0.0630	0.0003
	9	0.1197	1.9602	0.9047	0.0635	0.0004	0.0633	0.0004
	10	0.1204	1.9602	0.9041	0.0638	0.0004	0.0636	0.0004
05.00x10.00	0	0.1054	1.9602	0.9161	0.0676	0.0004	0.0674	0.0004
	1	0.1063	1.9602	0.9153	0.0678	0.0005	0.0677	0.0004
	2	0.1080	1.9602	0.9140	0.0685	0.0005	0.0683	0.0005
	...	...	...	...	...	...	...	...
	8	0.1155	1.9602	0.9080	0.0720	0.0008	0.0718	0.0007
	9	0.1161	1.9602	0.9075	0.0725	0.0009	0.0723	0.0008
	10	0.1166	1.9602	0.9071	0.0730	0.0009	0.0728	0.0008
05.00x07.50	0	0.1043	1.9602	0.9169	0.0696	0.0005	0.0695	0.0005
	1	0.1055	1.9602	0.9159	0.0700	0.0005	0.0698	0.0005
	2	0.1073	1.9602	0.9145	0.0707	0.0006	0.0706	0.0005
	...	...	...	...	...	...	...	...
	8	0.1149	1.9602	0.9086	0.0747	0.0009	0.0745	0.0008
	9	0.1155	1.9602	0.9081	0.0753	0.0010	0.0751	0.0009
	10	0.1159	1.9602	0.9077	0.0758	0.0011	0.0756	0.0010

A set of charts is plotted showing the performance for Barrel VRF of different configurations (Figure 5). It is divided vertically into seven different combinations of Roof/RRSM widths and lengths, and horizontally into five different rotational angles. Due to limited space, each rotational angle is divided into only 3 roof heights of 0.00, 5.00, and 10.00 m. For each chart, the x-axis represents hour of the day, and y-axis represents the Monthly Average Hourly Total Irradiance ($AHTI_{Monthly}$) and Monthly Average Hourly Energy Consumption ($AHEC_{Monthly}$), where significant differences are varying from one case to another. The next step is to realize the relative performance of different VRFs in relation to their corresponding flat roof as a benchmark for comparison, $AHTI_{Monthly}$ and $AHEC_{Monthly}$ are converted into $AHTI_{\%}$ and $AHEC_{\%}$ (Table 5) considering the following expressions by the authors:

$$AHTI_{\%} = \frac{(AHTI_{Monthly} - AHTI_{Monthly\ (Flat\ Roof)})}{AHTI_{Monthly\ (Flat\ Roof)}} \quad \text{Eqn. (1)}$$

$$AHEC_{\%} = \frac{(AHEC_{Monthly} - AHEC_{Monthly\ (Flat\ Roof)})}{AHEC_{Monthly\ (Flat\ Roof)}} \quad \text{Eqn. (2)}$$

This procedure will be repeated using (Equation 1) and (Equation 2) for determining VRFs that reduce the received solar radiation and consume less energy than their corresponding flat roof configuration. However, the results generally exhibit controversial effects where the solar irradiance decreases by increasing roof heights, while the energy consumption increases due to the increased internal volume, as can be seen in (Table 05). Therefore, there is need to recognize the VRFs' resulting total performance comprehensively. The last step includes summarizing the results by introducing the new Performance Index (PI) by the authors. It is based on a simple optimization technique, where the solar irradiance and energy consumption are realized simultaneously and standardized by converting their numerical values of different scales to a common one. This will prevent higher scales from having a larger influence on the estimation of PI. The $AHTI_{\%}$ are added to the standardized $AHEC_{\%}$ term to obtain PI value as an integrated indicator for the varying performance of different VRFs following this expression:

$$PI = AHTI_{\%} + \left(\left|\frac{AHTI_{max}}{AHEC_{max}}\right| . AHEC_{\%}\right) \quad \text{Eqn. (3)}$$

For example, for Barrel VRFs of rotational angle of 0° and different roof heights, the typical values of $AHTI_{\%}$ vary between 0.00 to 46.30%, while $AHEC_{\%}$ values vary between 8.76 to 0.00%. Using (Equation 3), the optimum performing VRF is having PI= -0.275, $AHTI_{\%}$= 40.72%, and $AHEC_{\%}$= 2.28%, while the worst case is having PI=0.00%, $AHTI_{\%}$= 43.86%, and $AHEC_{\%}$= 6.77%, as seen in (Figure 6). The variations of the standardized PI values and ranges imply their ability to express the relative importance of integrated metrics in the optimization procedure. The PI provides means for a VRF-to-VRF comparison under different geometrical configurations. It is worth mentioning that lower PI values indicate that a given VRF performs, on average, better than its corresponding flat roof, while VRFs of higher PI values are expected to receive larger amount of solar irradiance and consume more energy for cooling.

Table 5: Example of Barrel VRF Performance (Rotational Angle = 0.00) showing the Total $AHTI_{Monthly}$ and $AHEC_{Monthly}$ with their Corresponding Roof Widths, Lengths, and Heights, in addition to the $AHTI_{\%}$ and $AHEC_{\%}$ Compared to Flat Roof RRSM Performance

Roof Config.		$AHTI_{Monthly}$	$AHEC_{Monthly}$	$AHTI_{\%}$	$AHEC_{\%}$
W x L	H				
10.00x 10.00	0	71,388.18	16.80	0.00%	0.00%
	1	72,375.56	16.83	1.38%	0.17%
	2	66,726.88	16.88	6.53%	0.45%

	...	...	...	...	...
	8	40,949.78	17.35	42.64%	3.28%
	9	40,462.09	17.43	43.32%	3.74%
	10	40,077.12	17.51	43.86%	4.18%
10.00x07.50	0	71,388.18	17.44	0.00%	0.00%
	1	72,377.56	17.48	1.39%	0.25%
	2	66,726.83	17.55	6.53%	0.64%
	...	...	...	...	...
	8	40,949.78	18.14	42.64%	4.03%
	9	40,462.09	18.23	43.32%	4.55%
	10	40,077.12	18.32	43.86%	5.05%
05.00x10.00	0	71,388.18	19.42	0.00%	0.00%
	1	66,735.10	19.49	6.52%	0.37%
	2	47,805.39	19.67	33.03%	1.31%
	...	...	...	...	...
	8	38,889.56	20.68	45.52%	6.49%
	9	38,585.25	20.82	45.95%	7.23%
	10	38,337.29	20.96	46.30%	7.95%
05.00x07.50	0	71,388.18	20.02	0.00%	0.00%
	1	66,735.04	20.11	6.52%	0.48%
	2	47,805.39	20.33	33.03%	1.57%
	...	...	...	...	...
	8	38,792.12	21.46	45.66%	7.21%
	9	38,594.47	21.62	45.94%	8.00%
	10	38,337.29	21.77	46.30%	8.76%

The results of Barrel Vaults show that VRFs of rotational angle 135° obtained significant lower PI values than the other angles, particularly the ones of heights from 3 to 5 m. For example, 05.00x10.00 configuration with vault height of 3m and rotational angle of 135° (PI= -0.329) showed a significant decrease in both $AHTI_{\%}$ of 48.94% and $AHEC_{\%}$ of 2.33%. It is followed by 05.00x07.50 configuration with vault height of also 3m and rotational angle 135° (PI= -0.320) where it showed a noteworthy decrease in both $AHTI_{\%}$ of 48.96% and $AHEC_{\%}$ of 2.76%. While VRFs of rotational angle 45° tended to yield higher PI values than the other angles. For instance, 10.00x5.00 configuration with vault height of 5 m and rotational angle 45° (PI= -0.120) tended to be the least worst performing Barrel Vault as it yielded $AHTI_{\%}$ of 31.29% and $AHEC_{\%}$ of 3.92%, even though it had less PI value compared to other heights of that rotational angle. With regard to Pointed Vaults, it is apparent that VRFs of rotational angle 135° showed lower PI values than the other angles, also mainly the ones heights from 3 to 5m. For example, 05.00x10.00 configuration with vault height of 3 m and rotational angle of 135° (PI= -0.317) showed a significant decrease in both $AHTI_{\%}$ of 48.94% and $AHEC_{\%}$ of 2.33%. It is followed by 05.00x07.50 configuration with vault height of also 3 m and rotational angle 135° (PI= -0.306) where it showed a noteworthy decrease in both $AHTI_{\%}$ of 48.96% and $AHEC_{\%}$ of 2.76%. On the other hand, VRFs of rotational angle 45° tended to yield higher PI values than the other angles. For instance, 10.00x5.00 configuration with vault height of 6 m and rotational angle 45° (PI= -0.123) tended to be the least worst performing Pointed Vault, as it yielded $AHTI_{\%}$ of 38.68% and $AHEC_{\%}$ of 4.61%, yet it had less PI value compared to other heights of that rotational angle. Interestingly, the rest of VRFs followed the similar pattern, only with different values. Groin, Pointed Groin, Cloister, and Pointed Cloister Vaults of

rotational angle 135° showed lower PI values than the other angles, mostly for ones of heights from 3 to 5 m as well. For all of these VRFs, configuration 05.00x10.00 with vault height of 4 m and rotational angle of 135° (PI= -0.316 to -0.227) showed a significant decrease in both $AHTI_{\%}$ from 48.30 to 48.35% and $AHEC_{\%}$ from 2.68% to 2.78%. It is followed by 05.00x07.50 configuration with vault height of also 4 m and rotational angle 135° (PI= -0.301 to -0.224) where it showed a remarkable decrease in both $AHTI_{\%}$ from 48.23 to 48.33% and $AHEC_{\%}$ from 2.95 to 3.26%. In the same manner, VRFs of rotational angle 45° tended to yield unfavourably higher PI values than the other angles. For all of these four VRFs, 10.00x5.00 configuration with vault height of 4 m and rotational angle 45° (PI= -0.151 to -0.134) tended to be the least worst performing one, as it yielded $AHTI_{\%}$ of 28.66 to 23.52% and $AHEC_{\%}$ of 2.64 to 2.78%, yet it had less PI value compared to other heights of that rotational angle. In (Figure 6), the performance results of all VRFs with different configurations are summarized, emphasizing the reciprocal relationship between the solar irradiance received by these roofs and the resulting energy consumption simultaneously.

The convergence of the previous results interestingly encourages to deeply inspect the collective impact of Roof Heights, Rotational Angles, and VRF configurations on average solar irradiance and energy consumption. Using (Equation 1) and (Equation 2), the $AHTI_{\%}$ and $AHEC_{\%}$ of all VRFs are averaged and summarized in relation to the corresponding flat roofs, as seen in (Figure 7-a) and (Figure 7-b). The x-axis represents Roof Heights and Rotational Angles, respectively, while y-axis represents $AHTI_{\%}$ and $AHEC_{\%}$. Herein, regardless of Rotational Angle and VRF configurations, the relative performance of VRFs exhibited a contradicting behaviour with Roof Heights, divergent to previous results as seen in (Figure 7-a). Increasing roof heights from 0 to 10 m yielded an advantageous decrease in $AHTI_{\%}$ on average by 39.59 to 52.99% yet coupled with unfavorable increase in $AHEC_{\%}$ on average by 5.15 to 5.44%.

On the effect of Rotational Angle, regardless of Roof Height and VRF configurations, it can be concluded from (Figure 7-b) that VRFs of rotational angles 0°, 90°, 180° yielded an average decrease in $AHTI_{\%}$ by 46.77 to 48.18% yet coupled with a slightly better performance than other angles in $AHEC_{\%}$ by 5.15 to 5.24% on average. Although, VRFs of rotational angle 45° and 135° obtained a noteworthy decrease in $AHTI_{\%}$ on average, they also showed an increase in $AHEC_{\%}$ by 5.44% on average. Looking at the received solar irradiance and the resulting energy consumption simultaneously, VRFs of rotational angle 135° yielded the optimum performance compared to other angles. VRFs of rotational angle 45° obtained the lowest performance, with averaged $AHTI_{\%}$ and $AHEC_{\%}$ of 39.59% and 5.44% respectively.

Yet again, looking back into the previous results in (Figure 6), the performance of different VRFs were varying significantly from roof configuration to another, where they showed a tendency to be enhanced by decreasing Roof Widths. This is evident in configuration 05.00x10.00 that showed the best relative performance among other ones, followed by configurations 05.00x07.50; 07.50x10.0; 07.50x05.00; 10.00x10.00; 10.00x07.50; and 10.00x05.00. With regard to the effect of VRF types, (Figure 6) confirms

that $AHTI_{\%}$ and $AHEC_{\%}$ values fluctuate significantly from one type to another, especially when considering different roof heights, rotational angles. This suggests that acquiring a rule-of-thumb is complicated. However, to simplify the comparison, the best performing VRFs, those with heights from 3 to 5 m and orientation of 135° are evaluated here with regard to corresponding PI values, to detected significant performance differences. As shown in (Figure 6), Barrel Vaults showed the best performance compared to other types, with PI= -0.329, then Pointed Vaults with PI= -0.317. They were followed by Groin Vaults with PI= -0.316 and Pointed Groin Vaults with PI= -0.270. Lastly, Cloister Vaults with PI= -0.257, followed by Pointed Cloister Vaults that showed the worst performance of them all with PI= -0.227.

To sum things up, it can be concluded that VRFs configuration 05.00x10.00 of height from 3 to 4 m and orientation of 135° yielded the lowest amount of received solar irradiance and energy consumption simultaneously of all the investigated configurations. This was verified by minor PI values that ranged from -0.329 to -0.227, with reduced $AHTI_{\%}$ from 48.94 to 48.35% and reduced $AHEC_{\%}$ from 2.33 to 2.78% respectively. However, it is worth mentioning that the difference in $AHTI_{\%}$ and $AHEC_{\%}$ scales in (Figure 7-a) and (Figure 7-b) suggests that Roof Heights and Rotational Angles have diverse effects on the amount of the received solar irradiance and the resulting energy consumption. In this, by increasing Roof Heights, the decrease in the received solar irradiance occurs mainly due to the increase in the inclined angle of VRFs accompanied with an increase in self-shaded areas, while the increase in the energy consumption is owed to the increased internal volume of RRSM. However, how can the resulting dataset be used to extract and quantify significant associations among the study variables themselves in relation to different VRFs? This inquiry has not been yet fully answered and tackling it would require post-processing of the simulation results, providing a better understanding of the magnitude, distribution, and occurrence of the reciprocal relationship between solar irradiance and energy consumption and the study influencing variables.

The Second Phase: Principal Component Analysis

To uncover relationship patterns between the study variables and the simulation results, a conventional scatter plot matrix is created for the simulation results of Barrel VRF as an example. It shows plots for all the pairs of variables, where the x-axis represents the 11 independent variables, and y-axis represents dependent variables of AHTI and AHEC (Figure 8). Due to the complex interconnections between the variables in the multidimensional dataset, it is hard to extract important patterns from the independent and dependent variables, or even realize how they are related to each other by this traditional statistical method.

The unsupervised data reduction technique of Principal Components Analysis (PCA) (Jollife, I., 2010; Krzanowski, W., 2000) can be utilized to describe the variability of a multivariate dataset. By means of orthogonal transformations, PCA converts the dataset's possibly correlated variables into a set of linearly uncorrelated variables, called principal components, each of which represents a linear combination of the original variables. At that point, the data dimensionality reduction can be achieved by dropping the least

important principal components, while keeping the first few components that typically represent a higher variability of the original dataset, extracting as much information as possible. The principal components are then visualized by a two-dimensional plot to interpret the dataset variability. PCA follows a standard procedure to carry out such an analysis. Herein, PCA model is developed corresponding to the Pearson's correlation coefficient in XLSTAT, a Microsoft Excel's add-in created by Addinsoft. First, the XLSTAT standardizes the data numerical values to a comparable scale to prevent giving a false importance to larger values. Then, a correlation table is created (Table 6) by reporting a Pearson's correlation two tailed test, which determines the correlation between each variable and the simulation results. Decisions are made based on important correlations, not only from a statistical hypothesis testing perspective, but also from an architectural point of view. It is noticeable that the Roof Height, Cross-Sectional Ratio, and Compactness Ratio are highly correlated to AHTI. Also, RRSM Internal Volume, Thermal Envelope, and Roof External Area have an average correlation with AHTI. While Rotational Angle, Roof/RRSM Width, Roof/RRSM Length, RRSM Internal Area, and Roof Aspect Ratio have a low correlation with AHTI and could have been neglected without effecting the quality of the results. On the other hand, it is clear that RRSM Internal Area, RRSM Internal Volume, Thermal Envelope, and Compactness Ratio are highly correlated to AHEC. Also, Roof/RRSM Width, Roof/RRSM Length, and Roof External Area have an average correlation with AHEC. While Rotational Angle, Roof Height, Roof Aspect Ratio, and Cross-Sectional Ratio have a low correlation with AHEC, and could have been also removed from PCA without effecting the quality of the results. These preliminary results suggest that the received amount of solar irradiance is greatly influenced by the geometrical configurations of VRFs. However, the energy consumption is affected secondarily by roof forms, but rather mostly by the configurations of the space itself. It is also noted that the correlations of Rotational Angle with AHTI and AHEC are not high, and the reason behind this is owed to statistical and architectural explanations. Statistically, the correlation table examines the unconditional correlations between the study variables and results, depending on the data structure and size. The Rotational Angle shows a low correlation because it may be collinear by other variable or several ones in tandem, which in turn are correlated with the simulation results. This makes the Rotational Angle change from correlated to uncorrelated. Architecturally, the Rotational Angle has a low correlation with AHTI due to of the Earth's rotation, where the received solar irradiance in the northern-hemisphere changes rapidly throughout the day and differs also on a monthly or seasonal basis. Also, the established window configurations, which are set to be horizontal stripes on each wall (Table 2) to eliminate the effect of opening orientation and focus on the effect of roof form, minimize the impact of Rotational Angle on AHEC.

Table 6: The Correlation Table of the Study Influencing Independent and Dependent Variables

No.	Key Influencing Variables	AHTI	AHEC
(1)	Rotational Angle	-0.09	0.00
(2)	Roof Height	**-0.87**	0.06
(3)	Roof/RRSM Width	0.10	0.60
(4)	Roof/RRSM Length	0.02	0.62
(5)	RRSM Internal Area	0.10	**0.99**
(6)	RRSM Internal Volume	-0.53	**0.72**

(7)	Thermal Envelope	-0.54	**0.72**
(8)	Roof External Area	-0.46	0.43
(9)	Roof Aspect Ratio	-0.06	-0.09
(10)	RRSM Compactness Ratio	**0.68**	**-0.62**
(11)	Roof Cross-Sectional Ratio	**-0.79**	-0.19

Two variability charts (Figure 9) are then developed to demonstrate the quality of the data reduction from the 11-dimensional original dataset to a lower number of dimensions. They show the mathematical values that correspond to the amount of variability in the original data represented by magnitudes (Eigenvalues) (Figure 9-a) and directions (Eigenvectors) (Figure 9-b) of the resulting principal components. For instance, the eigenvalue of the first principal component is 4.846 representing 44.05% of the data variability. Thus, if the data is represented by one component, only 44.05% of the data would be explained. The sum of all eigenvalues equals the number of variables. Since the data was standardized, a principal component with an eigenvector near zero indicates that the corresponding variable contributes less to the component, whereas larger eigenvalue indicates that the corresponding variable contributes more to the component.

In the developed PCA model, the first two principal components account for a cumulative variability of 67.11% to explain the original data, providing a sufficient approximation of the relationships among most of the study's independent and dependent variables and how they are related to each other. These two components are plotted (Figure 10), where the variables are represented by vectors pointing away from the origin, while the angles between them approximate their inter-correlations. A small angle indicates a positive correlation, and an angle of 90 degrees shows that the variables are not correlated, while an angle close to 180 degrees designates a negative correlation. The length of the vector line and its closeness to the outer circle indicate how well the variables is represented. By visually inspecting the two-dimensional plot, interesting conclusions could be detected. A fair positive correlation is represented between AHTI and Compactness Ratio by the small angle between their two vectors. A stronger negative correlation between AHTI and Cross-Sectional Ratio, Roof Height, and Roof/RRSM Length is signified the by the larger angles between AHTI vector and other ones close to 180 degrees. On the other hand, A strong positive correlation between AHEC and RRSM Internal Area, RRSM Internal Volume, Thermal Envelope, and Roof External Area is noticed by the small angle between AHEC vector and other ones. A strong negative correlation is observed between AHEC and Compactness Ratio, confirmed by a large angle between their two vectors. However, there is not necessarily a direct interpretation to the principal components, since some information may be hidden in the poorly represented variables, and care must be taken when realizing the resulting plot. For example, Roof/RRSM Length is poorly represented here as indicated by the short length of its vector, since it is mostly associated with the third principal components (Figure 9-b). Likewise, the first two components did not account for the Rotational Angle in the plot as indicated by the shorter length of its vector, since it is well represented only by the fourth principal component (Figure 9-b). However, the effect of Rotational Angle can be realized only by considering its variations for individual VRFs of identical configurations. It is clear that those results comply with the preliminary findings of the correlation test (Table

6), supporting the conclusion that the received amount of solar irradiance is mainly influenced by the geometrical configuration of VRFs. However, in the case of energy consumption, the size of the internal spaces should primarily be taken into consideration.

Since the newly developed principal components represent combinations of the original dataset variability, interesting new features can be detected out of these transformations. The first principal component, represented by the x-axis, is strongly correlated with six independent variables, in addition to two dependent variables. It is proportional to Roof Height, RRSM Internal Area, RRSM Internal Volume, Thermal Envelope, Roof External Area, and AHEC, while it is inversely proportional to Compactness Ratio and AHTI. This correlation suggests that these variables vary together. For example, AHTI tends to increase by increasing the positively correlated variables, and by decreasing the remaining ones as well. In fact, the first principal component is strongly correlated with the Thermal Envelope, RRSM Internal Volume, Roof External Area, and Compactness Ratio, making it primarily a measure of the Compactness Ratio, where it is expressed by the other variables. Compactness Ratio is the ratio between the building's thermal envelope area and its internal volume, while, the Thermal Envelope is the area that separates the indoor environments from the outdoors. In this, it can be concluded that buildings in hot-arid regions that have VRFs of higher compactness ratio are less compact, as they have a larger thermal envelope in proportion to their volume. This would make them tend to have a larger amount of AHTI due to larger exposed surfaces to solar radiation, accompanied by a lower amount of AHEC due to lower internal volume, and vice versa. The second principal component, represented by the y-axis, is highly correlated with three independent variables and two dependent variables. It is positively proportional to Roof/RRSM Width, AHTI, and AHEC, while it is inversely proportional to Roof Aspect Ratio and Cross-Sectional Ratio. Therefore, this component can be viewed mainly as a measure of the concaveness of VRFs in terms of Cross-Sectional Ratio, since it is expressed by a diversification of the other two independent variables. In this, it can be concluded that buildings in hot-arid regions that have VRFs of higher cross-sectional ratio are more concave, and therefore have a larger self-shaded area. This means they would have a lower amount of AHTI due to larger shaded surfaces that are unexposed to solar radiation, accompanied by also a lower amount of AHEC due to lower internal dimensions, and vice versa.

Conclusions

This research blurs the demarcation between contemporary and traditional approaches, arising from the need to put forward passive solutions for reducing energy use for cooling and improving indoor thermal conditions in buildings. It is sought to eliminate the implied prejudices that often lead to miscomprehending the environmental treatments of traditional architecture. Those that are taken for granted as ideas architects think of, rather than ideas architects think with. In Egypt, with the heavy reliance on the generated electricity out of non-renewable resources, the major problem that the energy-sector encounters is the increasing energy demand, ultimately causing weather changes and irreversible deteriorations to the built

environment. While Egypt is a country of deep history and tradition, manifestations of its traditional architecture were lost. Existing Egyptian cities represent repetitions of building blocks, with no consideration to the local traditional techniques that used to prevent overheating and enhance the environmental performance. In this, many researchers have previously asserted the ability of domed roofs to significantly decrease the intensity of the received solar irradiance compared to flat roof surface, in the summer as well as in the winter as thoroughly reviewed in this paper. The work of this research expanded this endeavor and presented a comprehensive method investigating the thermal behaviour of six vaulted roof geometries, where the solar irradiance and energy consumption are realized simultaneously with reference to the hot-arid climate of Aswan, Egypt. The methodological procedure incorporated a simulation study, supported by the developed parametric algorithm, facilitated an automated generation of 2,310 cases of these VRFs rather than by direct manipulation. The integration between the computational simulation with the parametric modeling easily provided detailed performance quantifications of VRFs. The annual simulations were based on an hourly resolution, where the outputs were exploited to construct a large dataset covering 11 interconnecting explanatory variables. Although this approach may seem time-consuming, especially when a preliminary approximation is required, yet it signifies the implementation of performance-based methods at the early stages of design to obtain optimization, advancement and efficiency.

The simulations preliminary results suggested that the received amount of solar irradiance is mainly influenced by the geometrical configuration of VRFs. In the case of energy consumption, the size of the internal spaces should primarily be taken into consideration. The PCA showed even more interesting conclusions on how the study's independent and dependent variables were related together. It thoroughly disclosed the significant associations between the study independent (geometrical influencing variables) and dependent variables (the solar irradiance and energy consumption) by Pearson's Correlation and by Two-Dimensional Plot of the Principal Components. The final results were in good agreement with the preliminary findings of the correlation test, supporting that buildings in hot-arid regions that have VRFs of higher compactness ratio would tend to have a larger amount of solar irradiance due to larger exposed surfaces, accompanied by a lower amount of energy consumption due to lower internal volume. Buildings with more concave VRFs that have a larger self-shaded area receive lower amount of solar irradiance, accompanied by a minimized energy consumption due to lower internal dimensions. One of the major benefits of PCA lies in overcoming the issue of confounding, where a number of independent variables might be in collinearity with each other. This could be prevented by PCA that yields uncorrelated linear combinations of the original variables. Moreover, utilizing the principal components as regressors in future models might be better than using the original dataset directly, as they represent most of the data variability related to the dependent variables, reducing the risk of overfitting by estimating less input variables. The results of this study will contribute to the promotion of the use of curved roof forms and the adoption of vaulted roof forms in building energy codes and can be added to the Egyptian Code for Energy Efficiency in Buildings.

References

1. Abdel-Razek, R. H. (1998). **Factors Affecting Construction Quality in Egypt: Identification and Relative Importance**. Engineering, Construction and Architectural Management, 5(3), 220-227.
2. AlQadi, S. B., Sodagar, B., and Elnokaly, A. (2018). **Estimating the Heating Energy Consumption of the Residential Buildings in Hebron, Palestine. Journal of Cleaner Production**. 196, ISSN 0959-6526.
3. ANSI/ASHRAE Standard 140. (2011). **Standard Method of Test for the Evaluation of Building Energy Analysis Computer Programs**. American Society of Heating, Refrigerating, and Air-Conditioning Engineers.
4. Atlam, B. and Rapiea, A. (2016). Assessing the Future of Energy Security in Egypt. International Journal of Energy Economics and Policy. Vol, 6(4): 684-700.
5. Attia, S. (2010). **Zero Energy Retrofit: Case Study of a Chalet in Ain-Sukhna, Egypt**. In Proceedings of the American National Solar Energy Conference, Phoenix, Arizona.
6. Attia, S., and Wanas, O. (2012). **The Database of Egyptian Building Envelopes (DEBE): A Database for Building Energy Simulations**. Proceedings of the Fifth National Conference of IBPSA-USA (SimBuild 2012), Wisconsin, United States, 96-103.
7. Ayoub, M. (2016). **Associative Parametric Urbanism: A Computational Approach to Parameterization of Conceptual Design Phase**. In Proceedings of the 8th International Conference of the Arab Society for Computer Aided Architectural Design (ASCAAD), London, United Kingdom, pp. 207-216.
8. Ayoub, M., and Elseragy, A. (2018). **Parameterization of Traditional Domed-Roofs Insolation in Hot-Arid Climates in Aswan, Egypt**. Energy & Environment, 29(1), pp. 109 - 130.
9. Ballabio, D. (2015). **A MATLAB Toolbox for Principal Component Analysis and Unsupervised Exploration of Data Structure**. Chemometrics and Intelligent Laboratory Systems, 149, 1-9.
10. Becker, M., and Golay, P. (1999). **Rhino NURBS 3D Modeling**. New Riders, Indianapolis, United States.
11. Bowen, A. B. (1981). **Cooling Achievement in The Gardens of Moghul India**. In: Proceedings of the international passive and hybrid cooling conference, Florida, United States, Newark, Del: American Section of the International Solar Energy Society, pp.27-31.
12. Costanzo, V., Evola, G., Gagliano, A., Marletta, L., and Nocera, F. (2013). **Study on the Application of Cool Paintings for the Passive Cooling of Existing Buildings in Mediterranean Climates**. Advances in Mechanical Engineering, 5, 413675.
13. Costanzo, V., Yao, R., Essah, E., Shao, L., Shahrestani, M., Oliveira, A.C., Araz, M., Hepbasli, A. and Biyik, E. (2018). **A Method of Strategic Evaluation of Energy Performance of Building Integrated Photovoltaic in the Urban Context**. Journal of Cleaner Production, 184, 82-91.

14. Dogan, T., Reinhart, C. F., and Michalatos, P. (2014). **Automated Multi-Zone Building Energy Model Generation for Schematic Design and Urban Massing Studies**. In IBPSA eSim conference, Ottawa, Canada.
15. Egyptian Code of Energy Efficiency in Residential Buildings (EERB). (2008). ECP 306-2005, First Section (306/1). Ministry of Housing, Housing and Building National Research Center (HBRC), Egypt.
16. Egyptian Electricity Regulatory Authority (EERA). (2014). **Electricity Consumption Monthly Report Egyptian Electric Utility and Consumer Protection and Regulatory Unit**, Egypt ERA, 2014, Available at: http://egyptera.org/ar/elecreport.aspx.
17. Egyptian Ministry of Electricity and Energy (EMEE). (2012). **Egyptian Electricity Holding Company Annual Reports 2011-2012, Egyptian Electricity Holding Company**. Available at: http://www.moee.gov.eg/english new/report.aspx.
18. Elnokaly, A., and Elseragy A. (2006). **Revitalisation of Traditional Curved Roofs for Indoor Thermal Comfort in Hot Climates**. Proceedings of the 3rd International Conference; 2006; Cairo, Egypt.
19. Elnokaly, A., and Elseragy, A. (2007). **What Impedes the Development of Renewable Energy Technology in Egypt**. In: MCEET 2007 Sustainable Energy: Technologies, Materials and Environmental Issues, Cairo, Egypt.
20. Elnokaly, A., and Elseragy A. (2013). Sustainable heritage development: learning from urban conservation of heritage projects in non-western contexts, European Journal of Sustainable Development, Vol. 2, No. 1. ecsdev.org
21. Elnokaly, A., Elseragy, A., and Gamal, M. (2008) **A Proposal for an Ecological Park Towards a Sustainable Humane Habitat in Abu Qir, Alexandria, Egypt**. Proceedings of the 10th International Conference on Humane Habitat (ICHH), Mumbai, India.
22. Elseragy, A. (2003). **Architectural and Solar Potential of Curved and Flat Roofs in Hot Arid Regions, With Reference to Egypt**. PhD Thesis, University of Nottingham, Nottingham, United Kingdom.
23. Elseragy, A., and Elnokaly, A. (2007). **Assessment Criteria for Form Environmental Performance of Building-Envelope in Hot Climatic Regions**. In Proceedings of the Passive and Low Energy Architecture 24th International Conference PLEA 2007, Singapore, Republic of Singapore, pp.156-162.
24. Elseragy, A., and Elnokaly, A. (2008). **Proposal of Sustainable and Eco-Exurban Communities at The Western Desert Development Corridor in Egypt**. In Proceedings of CSAAR 2008, Instant Cities: Emergent Trends in Architecture and Urbanism in the Arab World, April 2008, Sharjah, UAE. Publication Press.

25. Elseragy, A., and, Gadi, M. (2003a) **Computer Simulation of Solar Irradiance Received by Curved Roof in Hot-Arid Regions**. Proceedings of the 3rd International Conference, Eindhoven, Netherlands.
26. Elseragy A, and Gadi, M. (2003b). **Sustainable Potentialities of Traditional Roofs Geometries in Egypt and Hot-Arid Climates, An Analytical Study of Traditional Curved-Roof Forms Towards More Energy Efficient Architecture**. Proceedings of the Passive and Low Energy Architecture 20th International Conference (PLEA2003), Santiago, Chile.
27. Faghih, A. K., and Bahadori, M. N. (2011). **Thermal Performance Evaluation of Domed Roofs**. Energy and Buildings, 43(6), 1254-1263.
28. Fahmy, M. (2010). **Interactive Urban Form Design of Local Climate Scale in Hot Semi-Arid Zone**. PhD thesis, School of Architecture, The University of Sheffield.
29. Fahmy, M., Mahdy, M., and Nikolopoulou, M. (2014). **Prediction of Future Energy Consumption Reduction Using GRC Envelope Optimization for Residential Buildings in Egypt**. Energy and Buildings, 70, 186-193.
30. Fathy, H. (1986). **Natural Energy and Vernacular Architecture: Principles and Examples with Reference to Hot Arid Climates**. United States: University of Chicago Press.
31. Gómez-Muñoz, V. M., Porta-Gándara, M. Á., and Heard, C. (2003). **Solar Performance of Hemispherical Vault Roofs. Building and Environment**, 38(12), 1431-1438.
32. Hadavand, M., and Yaghoubi, M. (2008). **Thermal Behavior of Curved Roof Buildings Exposed to Solar Radiation and Wind Flow for Various Orientations**. Applied Energy, 85(8), 663-679.
33. Jakubiec, A. and Reinhart, C.F. (2011). **Diva 2.0: DIVA-FOR-RHINO 2.0: Environmental Parametric Modeling in Rhinoceros/Grasshopper Using Radiance, Daysim and EnergyPlus**. Proceedings of the 12th Conference of International Building Performance Simulation Association, Sydney, Australia, pp. 2202-2209.
34. Jollife, I. (2010). Principal component analysis. New York: Springer.
35. Ko, W. H., and Schiavon, S. (2017). **Balancing Thermal and Luminous Autonomy in the Assessment of Building Performance**. In Building Simulation Conference 2017, California, United States, pp. 1966-1973.
36. Koch-Nielsen, H. (2013). **Stay Cool: A Design Guide for The Built Environment in Hot Climates**. Routledge.
37. Koita, Y. (1981). **Comfort Attainment in Moghul Architecture**. In: Proceedings of the international passive and hybrid cooling conference, Florida, United States, Newark, Del: American Section of the International Solar Energy Society, pp.32-36.
38. Konya, A. (1980). **Design Primer for Hot Climate**. London, United Kingdom: The Architectural Press Ltd, pp.3–42.
39. Krzanowski, W. (2000). Principles of multivariate analysis. Oxford: Oxford University Press.

40. Lagios, K., Niemasz, J., and Reinhart, C.F. (2010). **Animated Building Performance Simulation (ABPS), Linking Rhinoceros/Grasshopper with Radiance/DAYSIM**. Proceedings of SimBuild, New York City, Unites States.
41. Mainstone, R. (1983). **Developments in Structural Form**. United States: M.I.T Press, pp.95-136.
42. Meyn, S. K., and Oke, T. R. (2009). **Heat Fluxes Through Roofs and Their Relevance to Estimates of Urban Heat Storage**. Energy and Buildings, 41(7), pp. 745-752.
43. Mourtada, A. (2009). **National Consultation Egypt Policies for Energy Efficiency in Buildings in Egypt Energy Efficiency Codes in The Policy Mix**. JCEE, MED-ENEC, Cairo. [online]. Available at: http://www.jceeeg.net/download.asp?path=library/NC%20Building%20energy%20Egypt%2009%20report%20090615.doc.
44. Okba, E. M. (2005). **Building Envelope Design as a Passive Cooling Technique**. In Proceedings of Passive and Low Energy Cooling for the Built Environment, Santorini, Greece, pp. 467-474.
45. Olgyay, V. (1973). **Design with Climate**. Princeton, NJ: Princeton University Press, p.7.
46. Pearlmutter, D. (1993). **Roof Geometry as a Determinant of Thermal Behaviour: A Comparative Study of Vaulted and Flat Surfaces in a Hot-Arid Zone**. Architectural Science Review, 36(2), 75-86.
47. Ramamurthy, P., Sun, T., Rule, K., and Bou-Zeid, E. (2015). **The Joint Influence of Albedo and Insulation on Roof Performance: An Observational Study**. Energy and Buildings, 93, pp. 249-258.
48. Robinson, D., and Stone, A. (2004). **Irradiation modelling made simple: the cumulative sky approach and its applications**. Proceedings of the Passive and Low Energy Architecture 21th International Conference PLEA2004, The Netherlands, pp. 19-22.
49. Santamouris, M., and Asimakopoulos, D. (Eds.). (1996). **Passive Cooling of Buildings**. London; James & James.
50. Santamouris, M., Synnefa, A., and Karlessi, T. (2011). **Using Advanced Cool Materials in the Urban Built Environment to Mitigate Heat Islands and Improve Thermal Comfort Conditions**. Solar Energy, 85(12), pp. 3085-3102.
51. Sirimanna, M. P. G., and Attalage, R. A. (2016). **A Model for Analyzing the Thermal Performance of Roof Configurations with Flat Inclined Surfaces**. Energy and Buildings, 116, 122-132.
52. Soleimani, Z., Calautit, J. K., and Hughes, B. R. (2016). **Computational Analysis of Natural Ventilation Flows in Geodesic Dome Building in Hot Climates**. Computation, 4(3), 31.
53. Tang, R., Meir, I. A., and Etzion, Y. (2003a). **An Analysis of Absorbed Radiation by Domed and Vaulted Roofs as Compared with Flat Roofs**. Energy and buildings, 35(6), 539-548.
54. Tang, R., Meir, I. A., and Etzion, Y. (2003b). **Thermal Behavior of Buildings with Curved Roofs as Compared with Flat Roofs**. Solar energy, 74(4), 273-286.

55. Tedeschi, A., and Andreani, S. (2014). **AAD, Algorithms-Aided Design: Parametric Strategies Using Grasshopper**. Le Penseur Publisher, Potenza, Italy.
56. U.S. Green Building Council (USGBC). (2019). **Daylight**. Retrieved from https://www.usgbc.org/credits/healthcare/v4-draft/eqc-0
57. Ward, G.J. (1994). **The Radiance Lighting Simulation and Rendering System**. ACM: New York, NY, United States, pp. 459-472.
58. Winkelmann, F. C. (2001). **Modeling Windows in EnergyPlus**. In Proceedings of the 7th Conference of the International Building Performance Simulation Association (IBPSA), Rio de Janeiro, Brazil, pp. 457-464.
59. Zerefos, S. C., Tessas, C. A., Kotsiopoulos, A. M., Founda, D., and Kokkini, A. (2012). **The Role of Building Form in Energy Consumption: The Case of a Prismatic Building in Athens**. Energy and buildings, 48, 97-102.
60. Zeng, R., Wang, X., Di, H., Jiang, F., and Zhang, Y. (2011). **New Concepts and Approach for Developing Energy Efficient Buildings: Ideal Specific Heat for Building Internal Thermal Mass**. Energy and Buildings, 43(5), pp. 1081-1090.

Parametric Investigation of Traditional Vaulted Roofs in Hot-Arid Climates

Highlights:

- The research seeks to enhance the indoor thermal comfort in Hot-Arid regions.
- A parametric approach is used to derive annual simulations.
- Vaulted roofs with varying cross-section ratios and orientations are investigated.
- Optimized forms with minimum quantity of received solar irradiance are concluded.

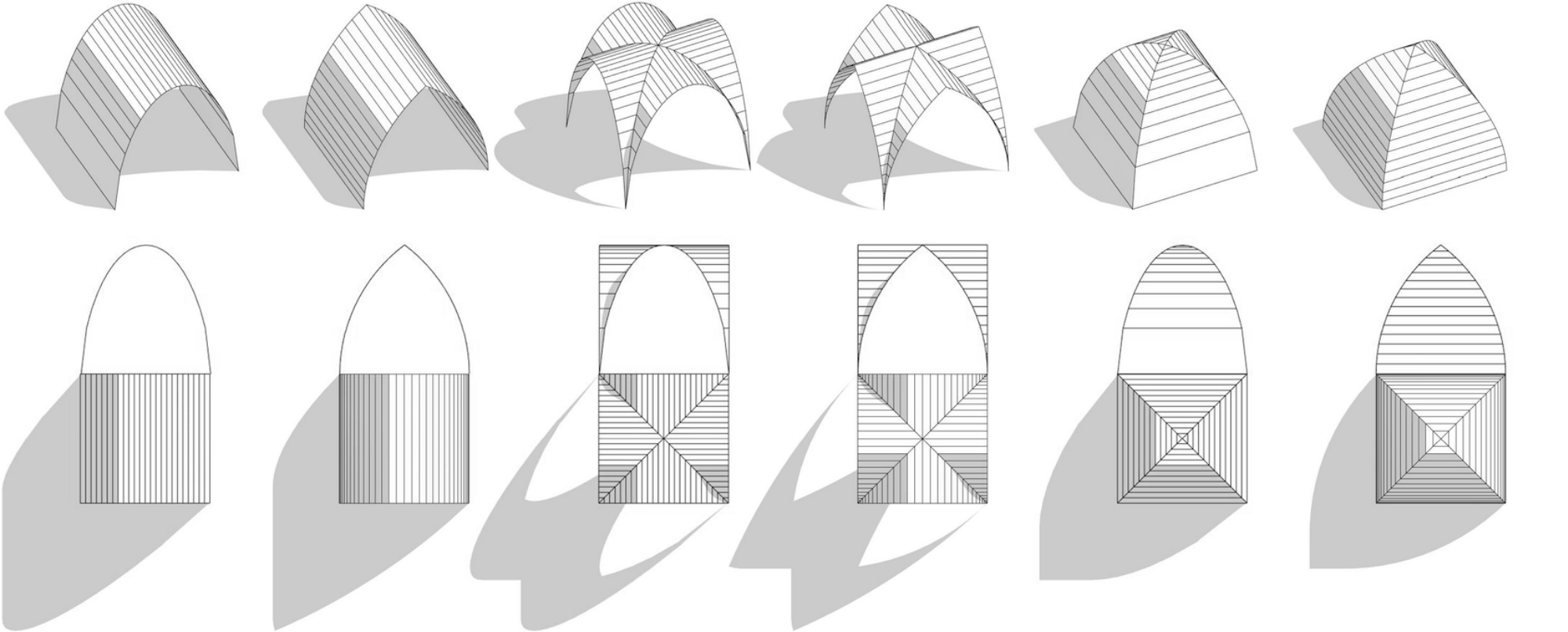
1. Barrel Vault
2. Pointed Vault
3. Groin Vault
4. Pointed Groin Vault
5. Cloister Vault
6. Pointed Cloister Vault

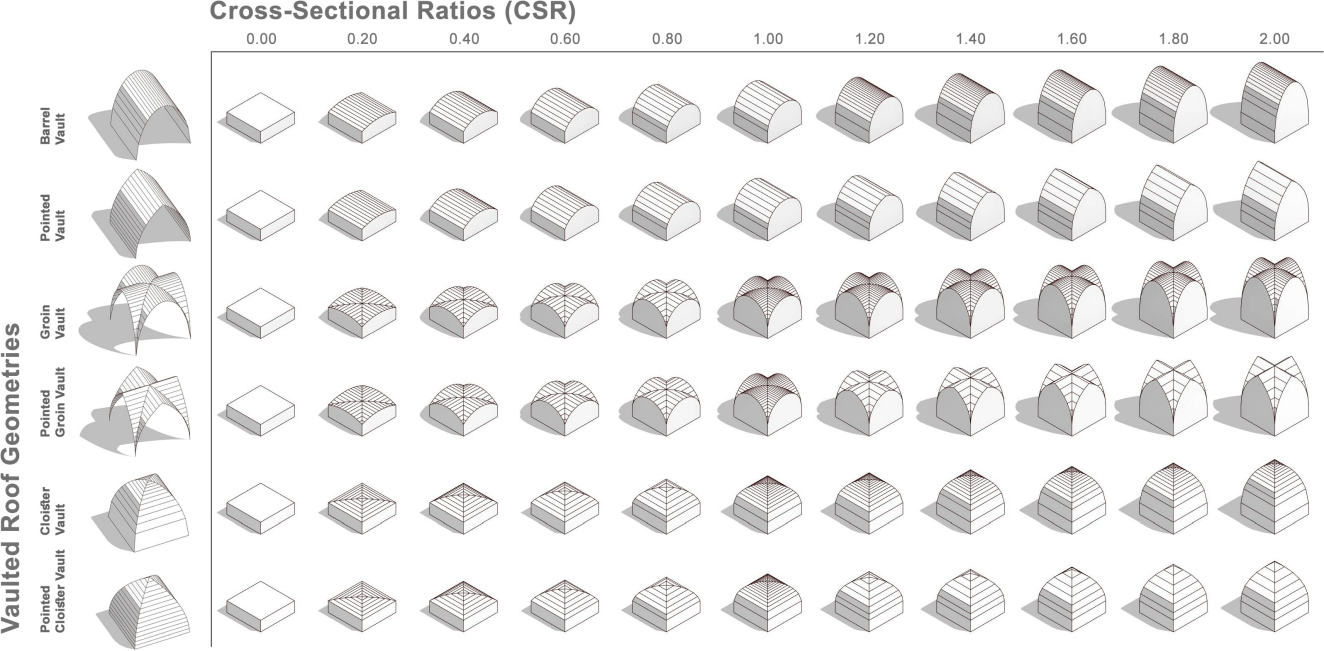
Cross-Sectional Ratios (CSR)
0.00
0.20
0.40
0.60
0.80
1.00
1.20
1.40
1.60
1.80
2.00
Vaulted Roof Geometries
Barrel Vault
Pointed Vault
Groin Vault
Pointed Groin Vault
Cloister Vault
Pointed Cloister Vault

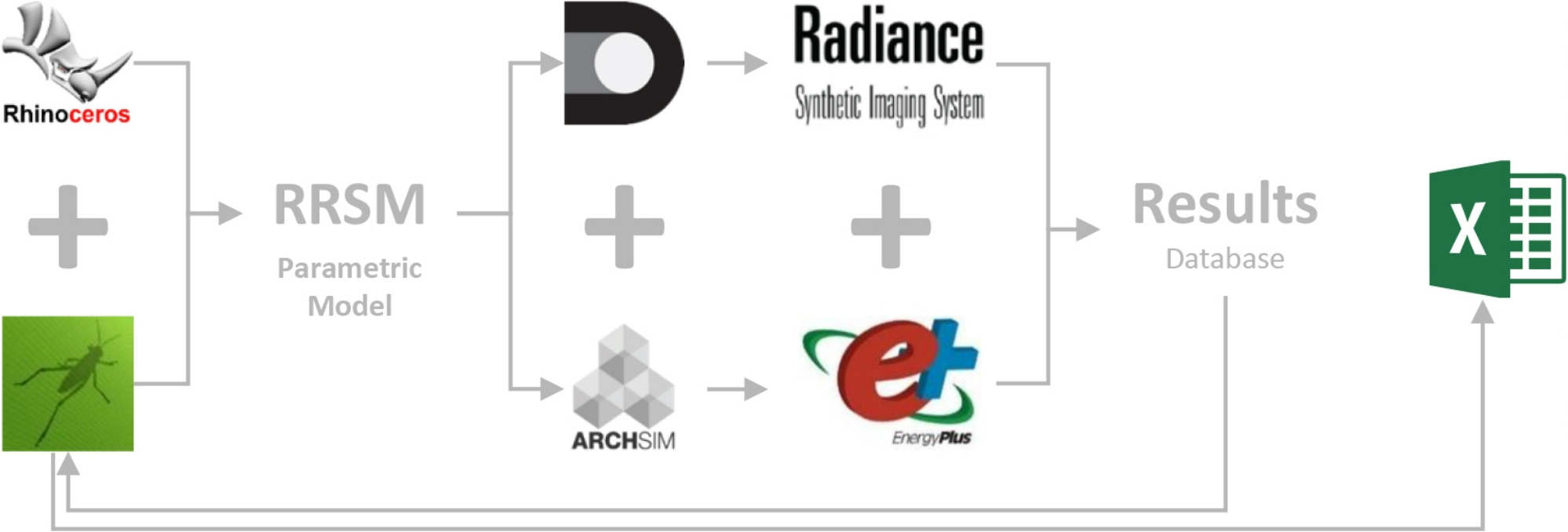
Rhinoceros
RRSM
Parametric
Model
Radiance
Synthetic Imaging System
ARCHSIM
EnergyPlus
Results
Database

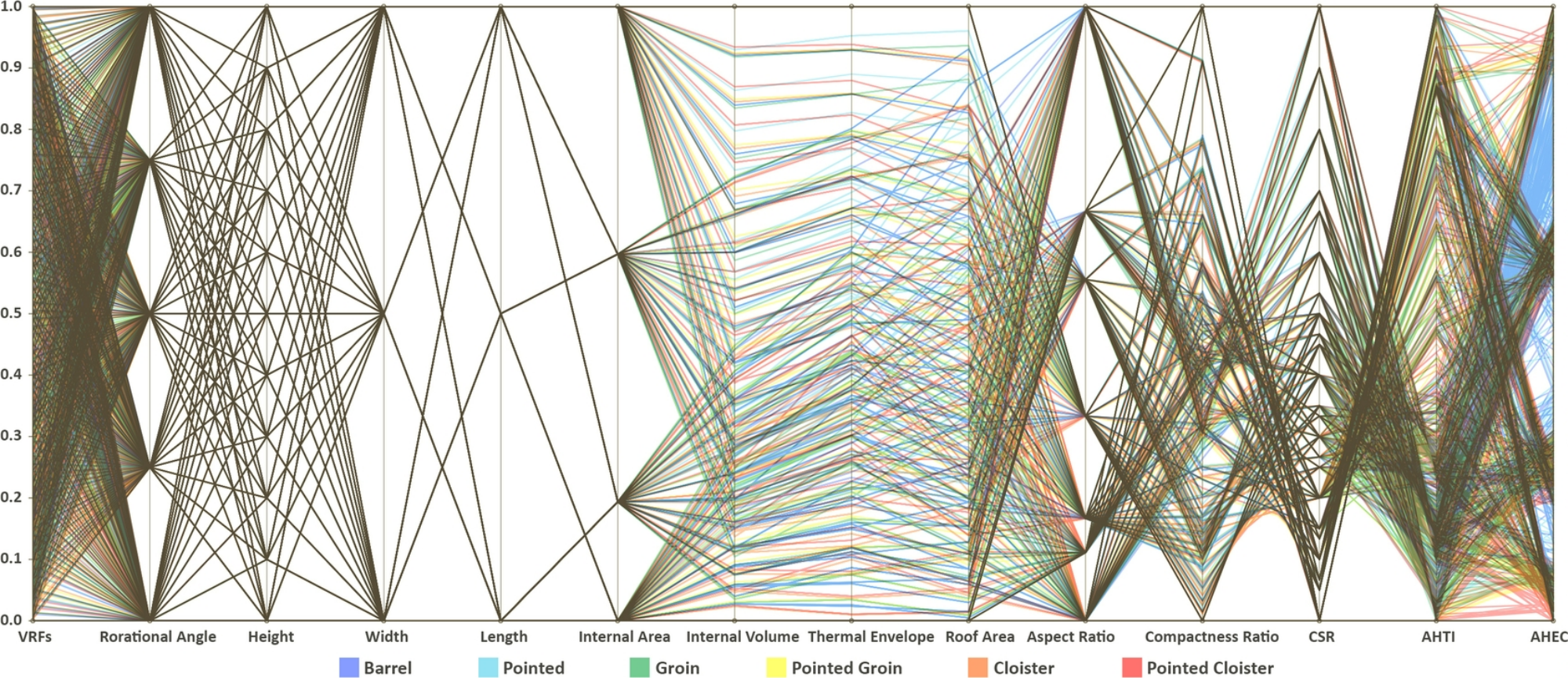
1.0
0.9
0.8
0.7
0.6
0.5
0.4
0.3
0.2
0.1
0.0
VRFs
Rorational Angle
Height
Width
Length
Internal Area
Internal Volume
Thermal Envelope
Roof Area
Aspect Ratio
Compactness Ratio
CSR
AHTI
AHEC
Barrel
Pointed
Groin
Pointed Groin
Cloister
Pointed Cloister

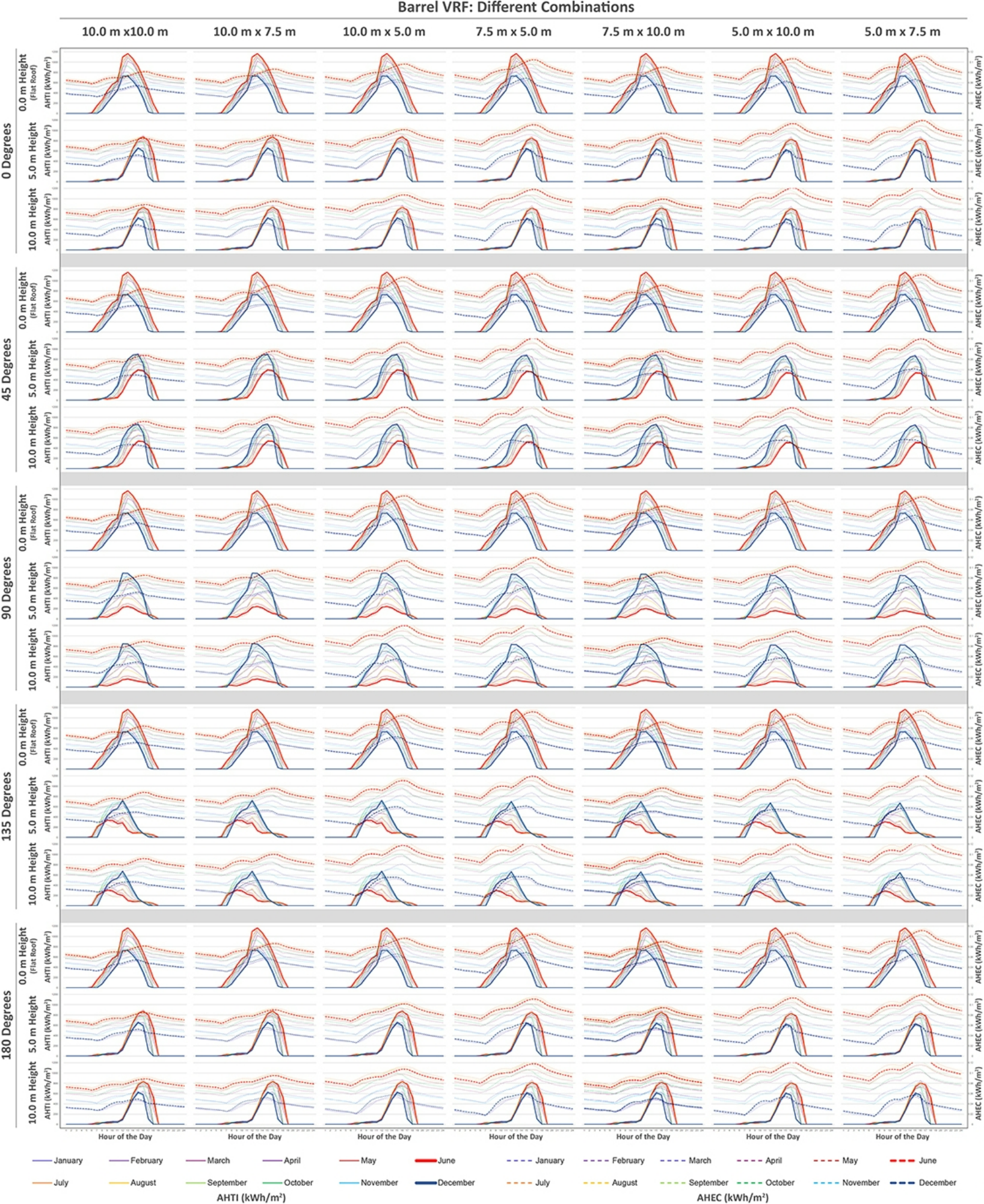
Barrel VRF: Different Combinations
10.0 m x10.0 m
10.0 m x 7.5 m
10.0 m x 5.0 m
7.5 m x 5.0 m
7.5 m x 10.0 m
5.0 m x 10.0 m
5.0 m x 7.5 m
0 Degrees
45 Degrees
90 Degrees
135 Degrees
180 Degrees
0.0 m Height (Flat Roof)
5.0 m Height
10.0 m Height
AHTI (kWh/m²)
AHEC (kWh/m²)
Hour of the Day
January
February
March
April
May
June
July
August
September
October
November
December
AHTI (kWh/m²)
AHEC (kWh/m²)

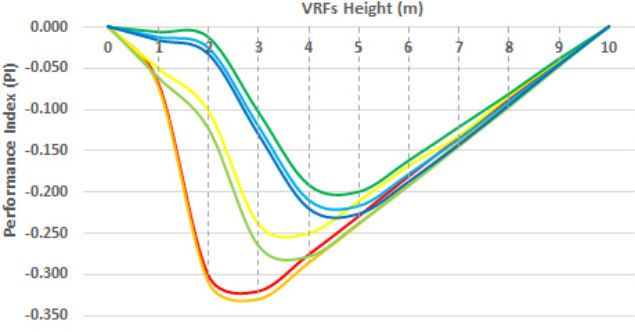

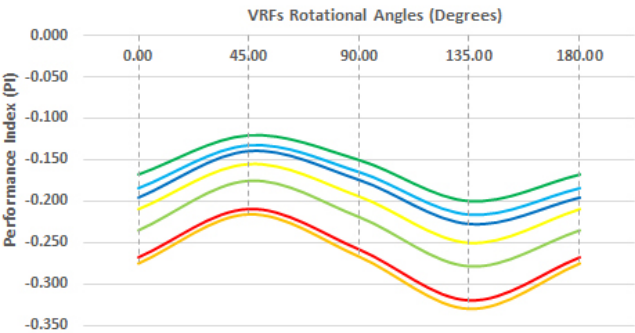

Barrel VRFs

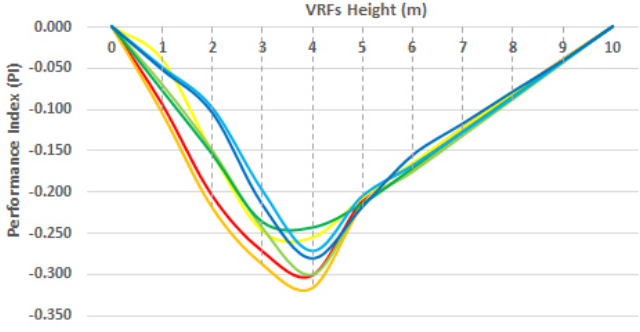

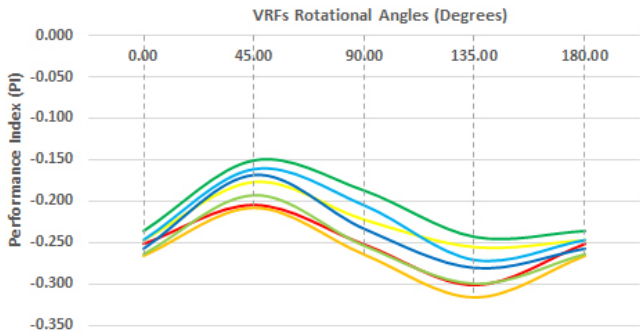

Groin VRFs

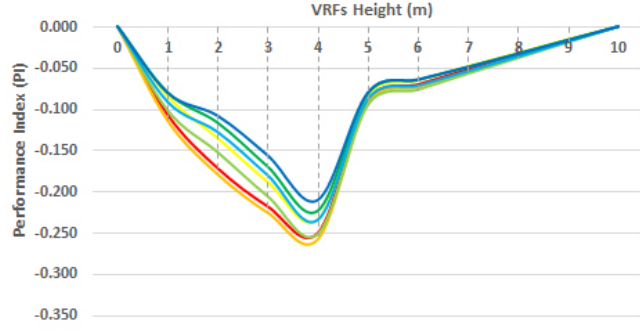

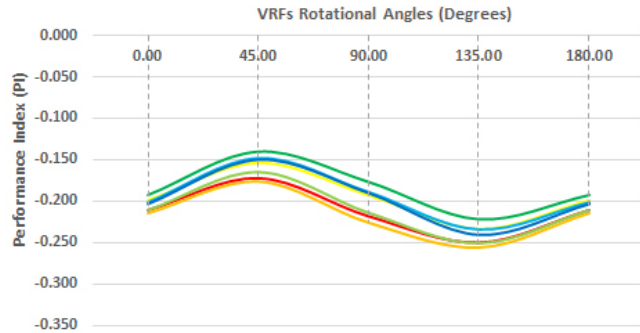

Cloister VRFs

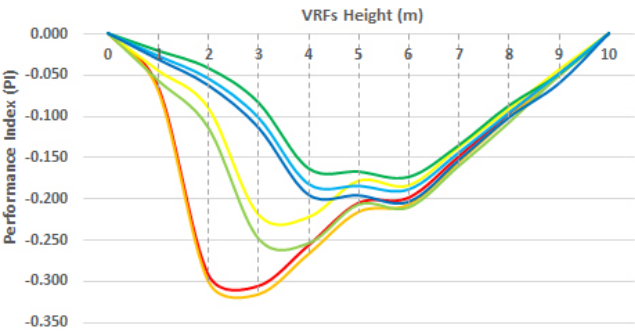

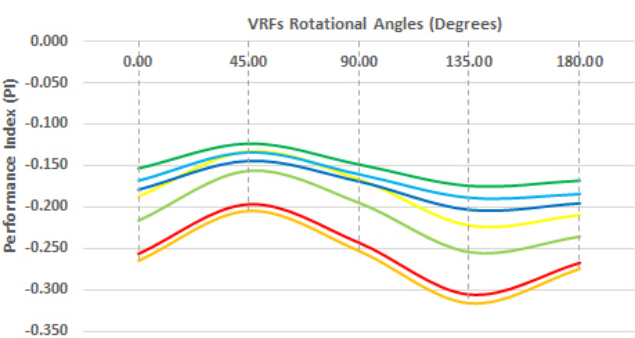

Pointed VRFs

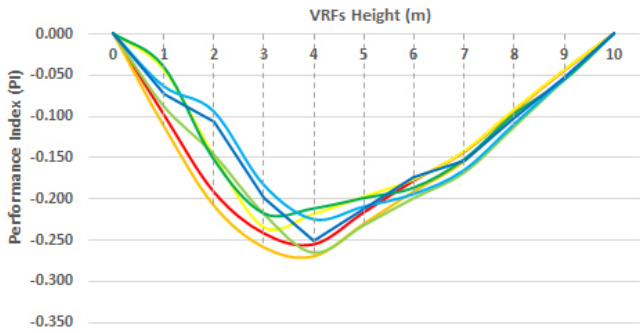

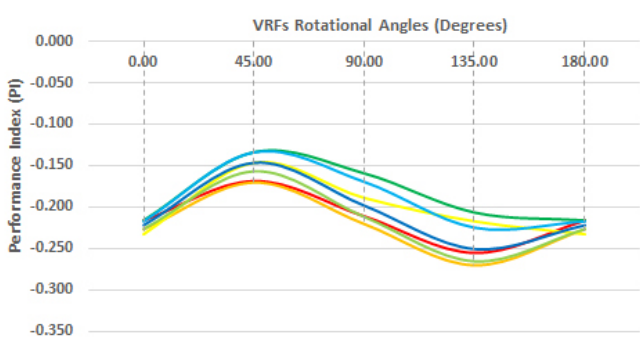

Pointed Groin VRFs

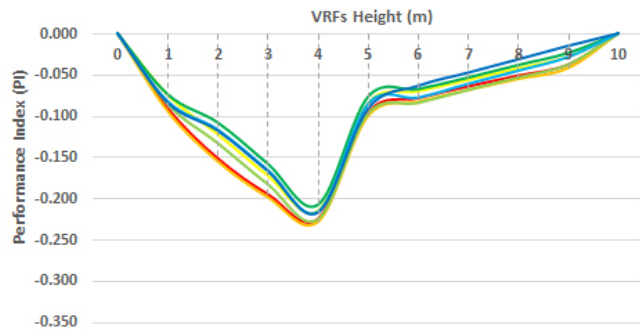

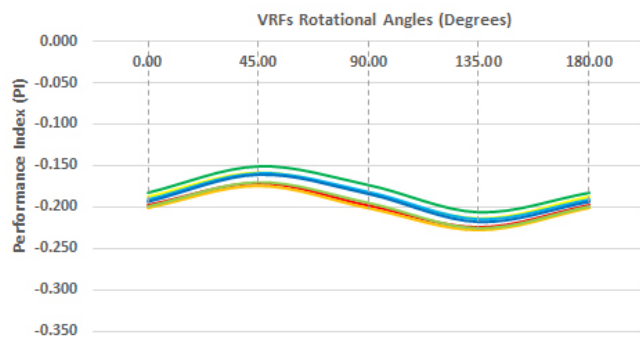

Pointed Cloister VRFs

05.00_07.50 05.00_10.00 07.50_05.00 07.50_10.00 10.00_05.00 10.00_07.50 10.00_10.00

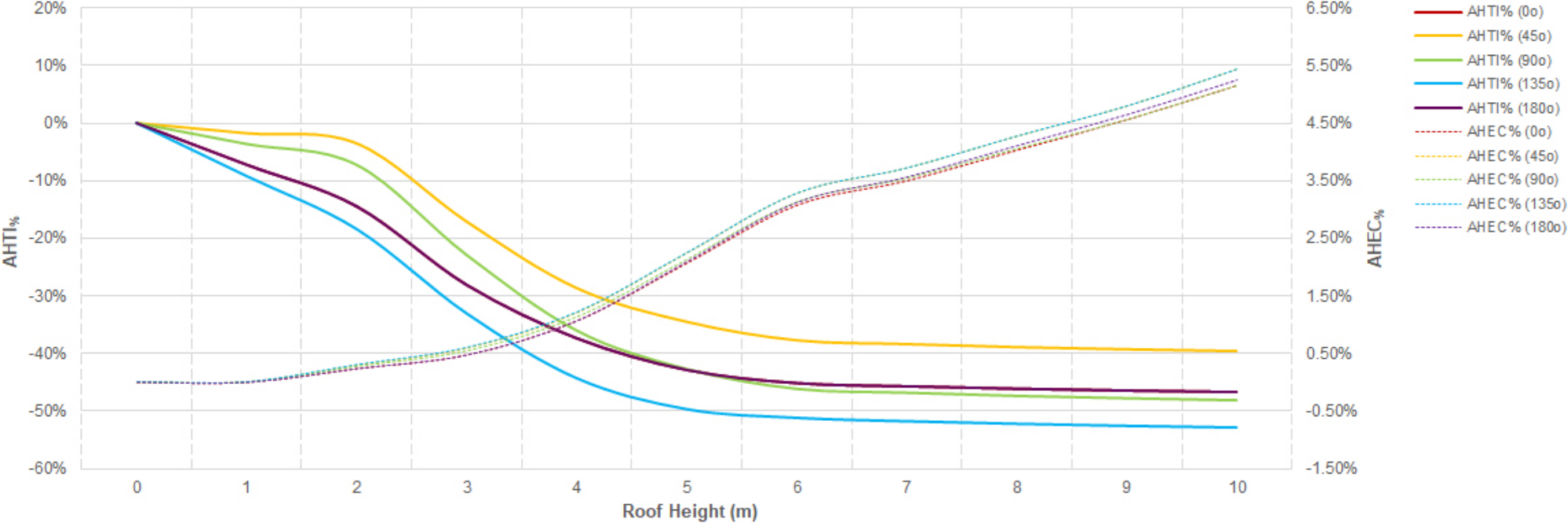
20%
10%
0%
-10%
-20%
-30%
-40%
-50%
-60%
AHTI%
6.50%
5.50%
4.50%
3.50%
2.50%
1.50%
0.50%
-0.50%
-1.50%
AHEC%
0
1
2
3
4
5
6
7
8
9
10
Roof Height (m)
AHTI% (0o)
AHTI% (45o)
AHTI% (90o)
AHTI% (135o)
AHTI% (180o)
AHEC% (0o)
AHEC% (45o)
AHEC% (90o)
AHEC% (135o)
AHEC% (180o)

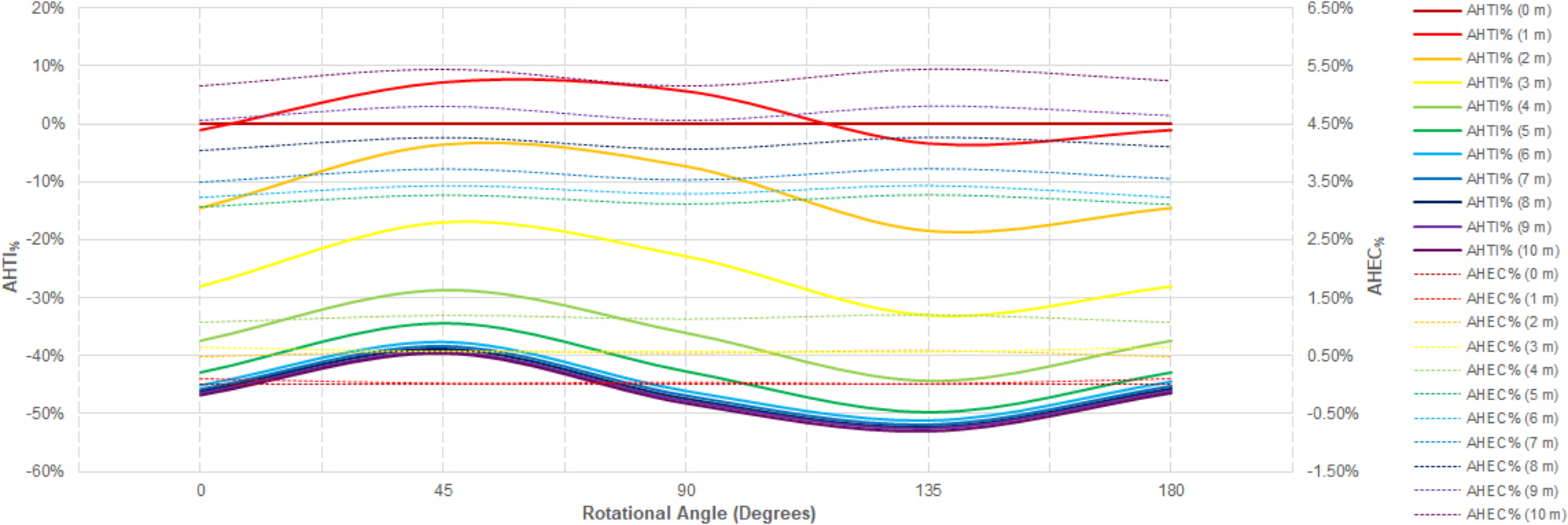
20%
10%
0%
-10%
-20%
-30%
-40%
-50%
-60%
AHTI%
6.50%
5.50%
4.50%
3.50%
2.50%
1.50%
0.50%
-0.50%
-1.50%
AHEC%
0
45
90
135
180
Rotational Angle (Degrees)
AHTI% (0 m)
AHTI% (1 m)
AHTI% (2 m)
AHTI% (3 m)
AHTI% (4 m)
AHTI% (5 m)
AHTI% (6 m)
AHTI% (7 m)
AHTI% (8 m)
AHTI% (9 m)
AHTI% (10 m)
AHEC% (0 m)
AHEC% (1 m)
AHEC% (2 m)
AHEC% (3 m)
AHEC% (4 m)
AHEC% (5 m)
AHEC% (6 m)
AHEC% (7 m)
AHEC% (8 m)
AHEC% (9 m)
AHEC% (10 m)

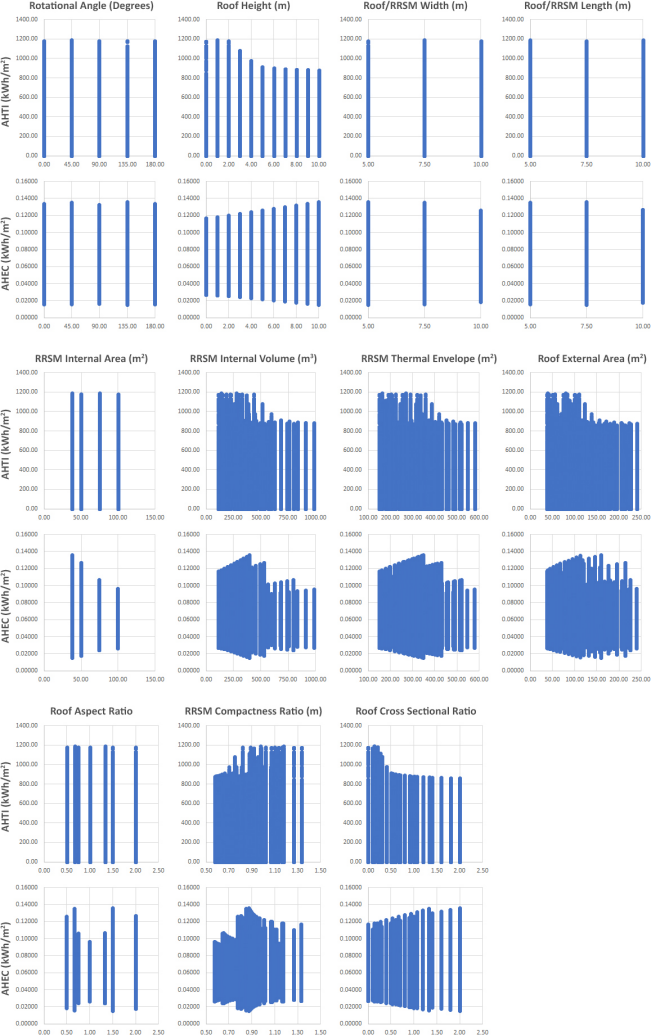
Rotational Angle (Degrees)
Roof Height (m)
Roof/RRSM Width (m)
Roof/RRSM Length (m)
AHTI (kWh/m²)
AHEC (kWh/m²)
RRSM Internal Area (m²)
RRSM Internal Volume (m³)
RRSM Thermal Envelope (m²)
Roof External Area (m²)
Roof Aspect Ratio
RRSM Compactness Ratio (m)
Roof Cross Sectional Ratio

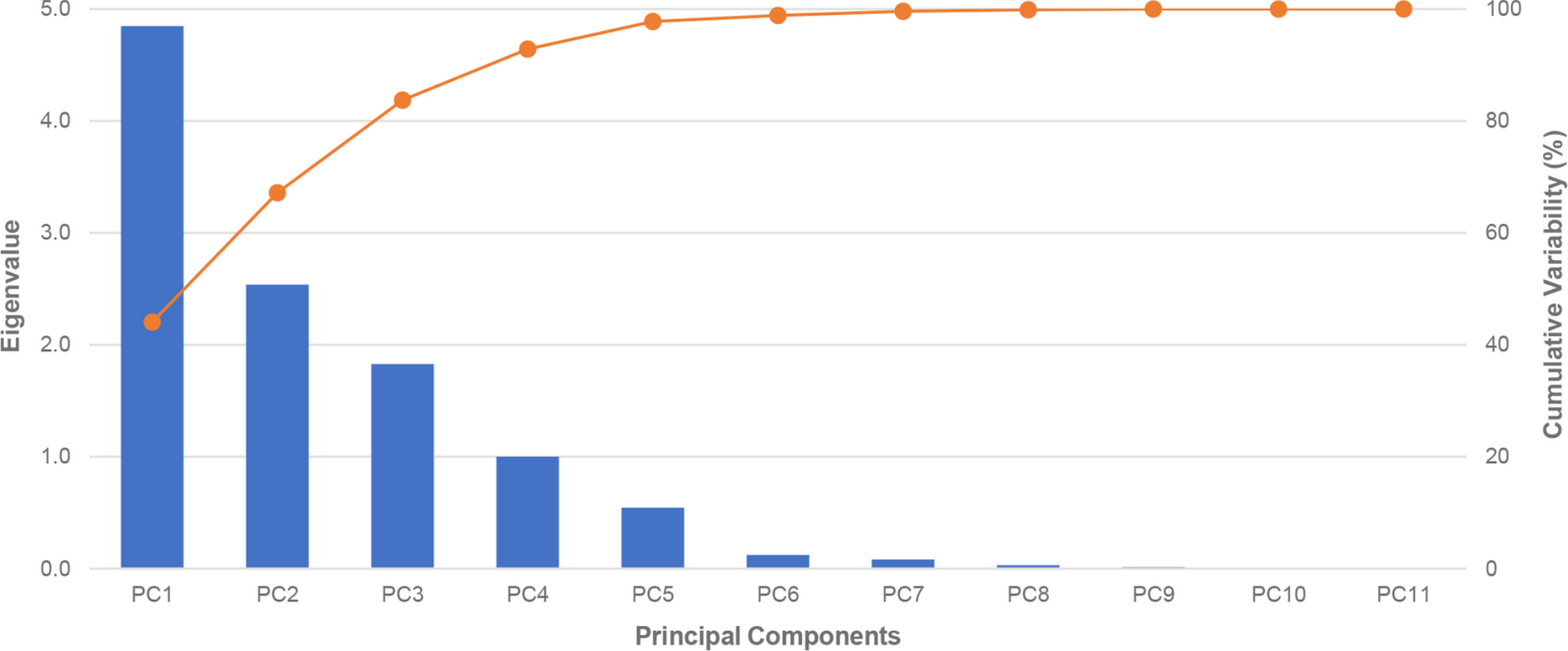
5.0
4.0
3.0
2.0
1.0
0.0
Eigenvalue
100
80
60
40
20
0
Cumulative Variability (%)
PC1
PC2
PC3
PC4
PC5
PC6
PC7
PC8
PC9
PC10
PC11
Principal Components

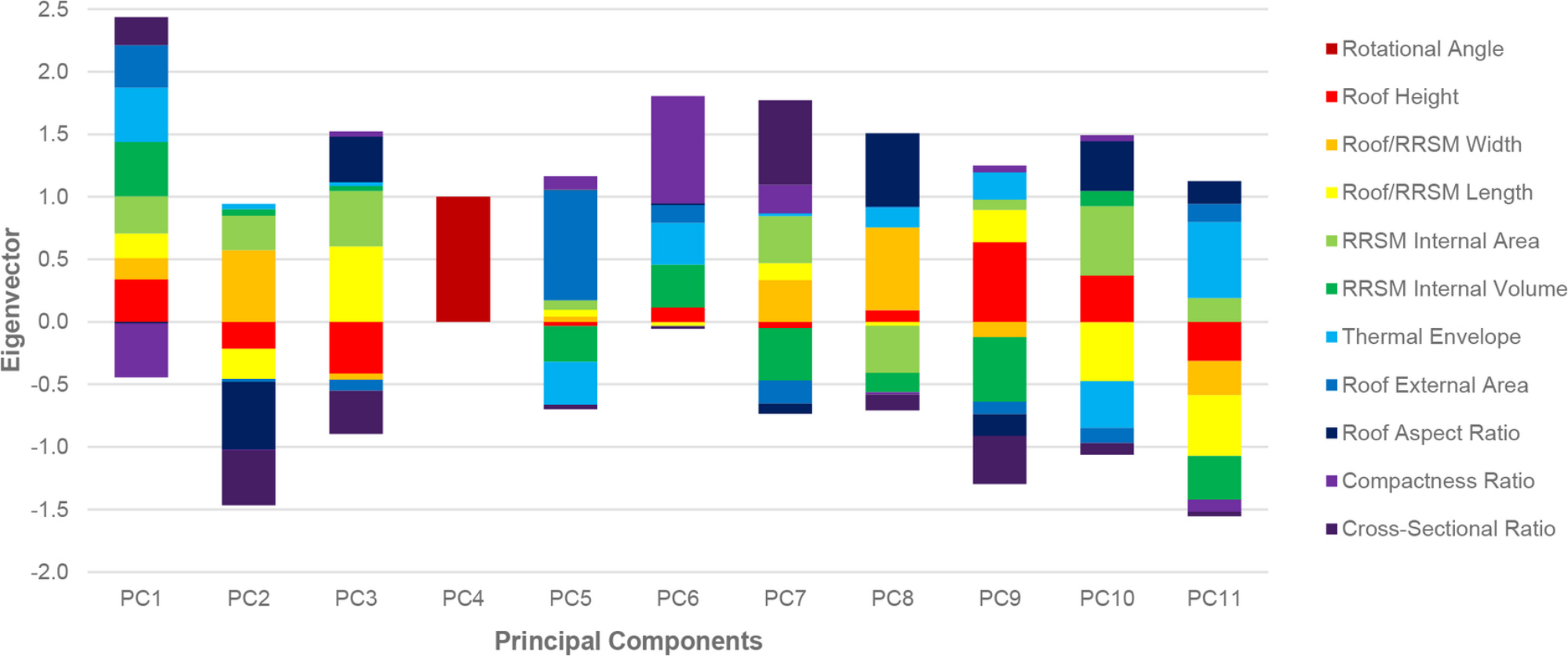
2.5
2.0
1.5
1.0
0.5
0.0
-0.5
-1.0
-1.5
-2.0
Eigenvector
PC1
PC2
PC3
PC4
PC5
PC6
PC7
PC8
PC9
PC10
PC11
Principal Components
Rotational Angle
Roof Height
Roof/RRSM Width
Roof/RRSM Length
RRSM Internal Area
RRSM Internal Volume
Thermal Envelope
Roof External Area
Roof Aspect Ratio
Compactness Ratio
Cross-Sectional Ratio

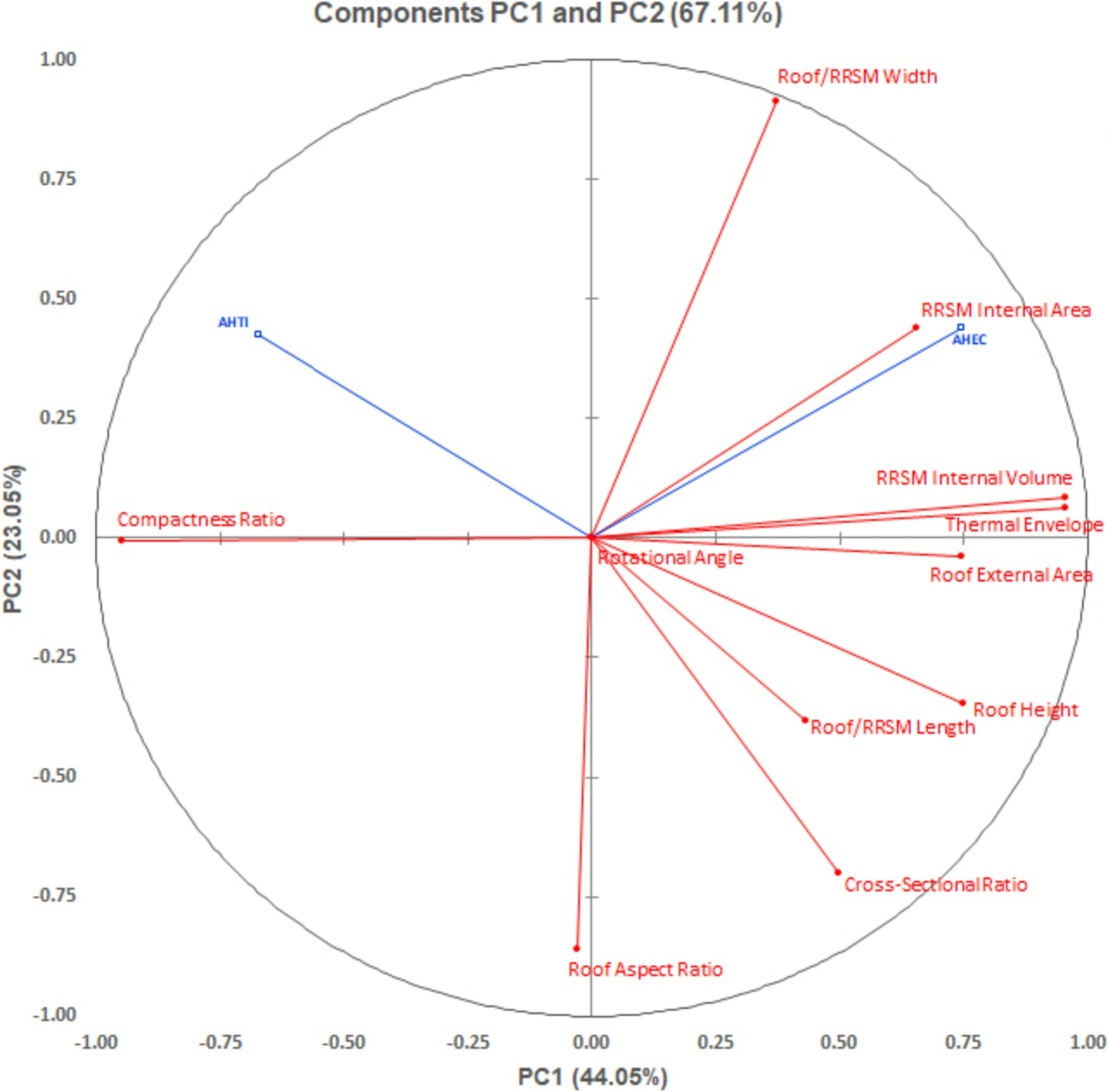
Components PC1 and PC2 (67.11%)
Roof/RRSM Width
RRSM Internal Area
AHTI
AHEC
RRSM Internal Volume
Compactness Ratio
Thermal Envelope
Rotational Angle
Roof External Area
Roof Height
Roof/RRSM Length
Cross-Sectional Ratio
Roof Aspect Ratio
PC2 (23.05%)
PC1 (44.05%)
1.00
0.75
0.50
0.25
0.00
-0.25
-0.50
-0.75
-1.00
-1.00
-0.75
-0.50
-0.25
0.00
0.25
0.50
0.75
1.00